Atomic Siegert states in a rotating electric field

Tor Kjellsson Lindblom,[1] Oleg I. Tolstikhin,[2] and Toru Morishita[1]
[1]*Institute for Advanced Science, The University of Electro-Communications, 1-5-1 Chofu-ga-oka, Chofu-shi, Tokyo 182-8585, Japan*
[2]*Moscow Institute of Physics and Technology, Dolgoprudny 141700, Russia*

(Received 31 May 2021; accepted 12 August 2021; published 25 August 2021)

We show that the time-dependent Schrödinger equation describing in the dipole approximation the interaction of a one-electron atom with a monochromatic circularly polarized electromagnetic field can be reduced to a stationary Schrödinger equation in the form which allows to separate variables in the asymptotic region and explicitly formulate outgoing-wave boundary conditions. The solutions to this equation are called atomic Siegert states (SSs) in a rotating electric field. We develop the theory of such states and propose an efficient method to construct them using powerful techniques of stationary scattering theory. The method yields not only the SS eigenvalue defining the Stark-shifted energy and total ionization rate of the state, but also the SS eigenfunction defining partial ionization amplitudes and the photoelectron momentum distribution. The theory is illustrated by calculations for a model potential.

DOI: 10.1103/PhysRevA.104.023110

I. INTRODUCTION

In strong-field physics [1], one deals with highly nonperturbative light-matter interaction processes for which the language of few-photon transitions becomes inadequate and novel theoretical approaches are required. The Keldysh theory [2] and its versions known as the strong-field approximation [3,4] suggest a general framework which has replaced standard time-dependent perturbation theory in treating strong-field processes. The physical picture underlying this approach is elucidated in the three-step model [5,6]. Its further elaborations are presented in the intense-field many-body S-matrix theory [7,8] and quantum orbit theory [9–11]. There also exist approaches based on different approximations. Thus, the time-dependent effective range theory [12,13] treats a simplified target model which allows advanced analytical description. The adiabatic theory [14] is an asymptotics which becomes exact in the low-frequency limit. Furthermore, there exist various Floquet approaches which were developed outside the three-step model paradigm but treat the same physical problem. This includes the quasistationary quasienergy states approach [15,16], non-Hermitian Floquet theory [17,18], high-frequency Floquet theory [19–21], R-matrix Floquet theory [22–25], and generalized Floquet formalisms [26–28]; see also Ref. [29] and references therein. Given that the numerical solution of the time-dependent Schrödinger equation (TDSE) even for one-electron atomic targets is still not a "solved" problem [30], theories based on suitable approximations remain helpful for understanding and predicting strong-field phenomena.

Theories which aim to be quantitative usually involve new technical elements whose implementation in practical calculations is decisive for applications. Consider, for example, the adiabatic theory [14], which is closer to the present context. In this theory, the solution to the TDSE and observables are obtained as asymptotic expansions in a small parameter given by the ratio of the electron and laser field timescales. In the leading-order approximation, strong-field ionization is treated as if the ionizing field were static and equal to the instantaneous laser field. All the results are therefore expressed in terms of properties of a Siegert state (SS) of the target in a static electric field, the one which originates from the unperturbed initial state as the field is turned on. To implement the theory, one needs to calculate the SS, which is a nontrivial computational task. Importantly, both the SS eigenvalue defining the Stark-shifted energy and ionization rate of the state and eigenfunction defining the transverse momentum distribution of electrons in the outgoing flux are needed. An efficient method to construct atomic [31] and molecular [32,33] SSs in a static electric field was developed. Armed with this method, the adiabatic theory quantitatively reproduces strong-field photoelectron momentum distributions (PEMDs) obtained by solving the TDSE [14,34–38] and in experiments [39–42], thus providing a reliable platform for studying strong-field processes in the adiabatic regime.

One can think of a theory in which strong-field observables are sought as asymptotic expansions in the ratio of the field period to the duration of a laser pulse, that is, in the inverse number of optical cycles in the pulse. Such a theory becomes exact for purely monochromatic fields, and hence its results should be expressed in terms of properties of the corresponding Floquet state. As in the adiabatic theory, one can expect that both the Floquet eigenvalue and eigenfunction are needed to obtain observables. In particular, PEMD should be determined by the behavior of the Floquet eigenfunction in the asymptotic region, where the outgoing flux of electrons released from the target by the field is formed. There exists a vast literature on the theory and computation of Floquet states [15–29]. However, most practical methods for solving the Floquet eigenvalue problem employ an approach pioneered

in Ref. [43] which is based on the dilatation transformation (complex coordinate method) followed by expanding the solution in a square integrable basis. This approach enables one to avoid the need of formulating outgoing-wave boundary conditions explicitly. It is efficient for calculating the Floquet eigenvalue, but constructing the Floquet eigenfunction in the asymptotic region of the real coordinate axis needed to obtain the PEMD in this approach is very difficult, if not impossible [44]. This difficulty hinders the development and potentially wide applications of the theory mentioned above.

To overcome this difficulty, a different approach to calculating Floquet states is needed. In the general case of a monochromatic field with arbitrary polarization, the Floquet eigenvalue problem for a one-electron target can be reduced to an infinite set of coupled time-independent three-dimensional (3D) equations for Floquet components [29]. These equations can be solved using powerful techniques of quantum scattering theory. Such an approach requires to explicitly formulate the outgoing-wave boundary conditions. Furthermore, if the original TDSE is written in the length or velocity gauges, the equations for Floquet components contain couplings induced by the interaction with the field which do not decay in the asymptotic region. This does not allow to separate variables and find an analytical solution for Floquet components in the asymptotic region which could be matched with a numerical solution in the inner region to obtain partial ionization amplitudes, in the spirit of scattering calculations. Thus, the scattering theory approach encounters its own difficulties: the need to treat an infinite set of coupled 3D equations and the problem of asymptotic couplings.

The latter difficulty can be resolved in the general case by transforming the TDSE to the Kramers-Henneberger (KH) coordinate frame [45,46]. The equations for Floquet components in the KH frame do not contain asymptotic couplings [29] and can be solved by scattering theory methods [47–51]. However, one still has to treat an infinite number of equations. The former difficulty can be eliminated in the special case of circularly polarized fields. In this case, by transforming the TDSE to a rotating coordinate frame, the Floquet eigenvalue problem can be reduced to a single time-independent equation [52,53]. This transformation was used in early studies of Floquet states supported by zero-range [54–56] and Coulomb [57,58] potentials in a circularly polarized field. However, equations considered in these studies still suffer from the problem of asymptotic couplings.

In this paper, we resolve *both* difficulties for the case of circularly polarized fields. We apply a composite coordinate frame transformation to the TDSE, first transforming it to the KH frame and then to a rotating frame. This enables us to reduce the Floquet eigenvalue problem to a single time-independent 3D equation which is free from the problem of asymptotic couplings. The resulting equation has the form of a stationary Schrödinger equation and is suitable for solving by scattering theory techniques. This equation occupies a special position in the theory of Floquet states. To emphasize this fact, we call its solutions atomic SSs in a rotating electric field. We develop the theory of such states and propose an efficient method to construct them in practical calculations. These developments pave the way to treating envelope effects in strong-field processes induced by finite circularly polarized pulses.

The paper is organized as follows. The theory of atomic SSs in a rotating electric field is presented in Sec. II. In Sec. III, we report calculations for a model potential illustrating the theory and the present computational method and discuss properties of the SSs needed for predicting strong-field observables. Section IV concludes the paper and gives an outlook for future research. Some technical details of the derivation in Sec. II are discussed in Appendices A and B. The numerical procedure used in the calculations is described in Appendix C.

II. THEORY

A. Time-dependent Schrödinger equation in the laboratory frame

We consider an electron whose coordinate relative to the laboratory (L) frame is denoted by $\mathbf{r}_{\rm L}$ interacting with an atomic potential $V(\mathbf{r}_{\rm L})$ and a homogeneous electric field $\mathbf{F}(t)$. The TDSE describing the system in the L frame reads as (atomic units are used throughout the paper)

$$i\frac{\partial\psi_{\rm L}(\mathbf{r}_{\rm L},t)}{\partial t}=\left[-\frac{1}{2}\Delta_{\rm L}+V(\mathbf{r}_{\rm L})+\mathbf{F}(t)\mathbf{r}_{\rm L}\right]\psi_{\rm L}(\mathbf{r}_{\rm L},t). \quad (1)$$

The potential is assumed to be axially symmetric about the $z_{\rm L}$ axis, $V(\mathbf{r}_{\rm L})=V(r_{\rm L},\theta_{\rm L})$, and satisfies

$$V(\mathbf{r}_{\rm L})|_{r_{\rm L}\to\infty}=-\frac{Z}{r_{\rm L}}-\frac{D\cos\theta_{\rm L}}{r_{\rm L}^2}+O\big(r_{\rm L}^{-3}\big), \quad (2)$$

where Z is the total charge of the parent ion and $\mathbf{D}=(0,0,D)$ is its dipole moment. The field remains constant in strength, $|\mathbf{F}(t)|=F$, and rotates with angular frequency ω in the $(x_{\rm L},y_{\rm L})$ plane:

$$\mathbf{F}(t)=F(\cos\omega t,\sin\omega t,0). \quad (3)$$

In the context of strong-field physics, Eq. (1) describes the interaction of an atom (or a linear molecule) treated in the single-active-electron approximation with a monochromatic circularly polarized electromagnetic field (propagating along the molecular axis) in the dipole approximation and length gauge. The interaction causes ionization of the atom. We are interested in the ionization observables.

We assume that in the absence of the field, $F=0$, the electron is in a bound state with energy E_0 and wave function $\phi_0(\mathbf{r}_{\rm L})$ defined by

$$\left[-\frac{1}{2}\Delta_{\rm L}+V(\mathbf{r}_{\rm L})-E_0\right]\phi_0(\mathbf{r}_{\rm L})=0. \quad (4)$$

The wave function has the form

$$\phi_0(\mathbf{r}_{\rm L})=\phi_0(r_{\rm L},\theta_{\rm L})\frac{e^{im_0\varphi_{\rm L}}}{\sqrt{2\pi}}, \quad (5)$$

where $\phi_0(r_{\rm L},\theta_{\rm L})$ is real, and is normalized by

$$\int|\phi_0(\mathbf{r}_{\rm L})|^2\,d\mathbf{r}_{\rm L}=\int_0^\infty\int_0^\pi\phi_0^2(r_{\rm L},\theta_{\rm L})r_{\rm L}^2\sin\theta_{\rm L}d\theta_{\rm L}dr_{\rm L}=1. \quad (6)$$

As the field is adiabatically turned on, $F > 0$, the bound state, being analytically continued in F, turns into a Floquet state

$$\psi_{\rm L}(\mathbf{r}_{\rm L}, t) = e^{-iE_{\rm L}t}\Phi(\mathbf{r}_{\rm L}, t), \tag{7}$$

where $\Phi(\mathbf{r}_{\rm L}, t) = \Phi(\mathbf{r}_{\rm L}, t + 2\pi/\omega)$ is a periodic function of time. The Floquet eigenvalue (or the quasienergy [29,59]) $E_{\rm L}$ is complex, its imaginary part defines the ionization rate of the state. The Floquet eigenfunction (or the dressed state [29]) $\Phi(\mathbf{r}_{\rm L}, t)$ satisfies outgoing-wave boundary conditions and its asymptotic form defines the PEMD. Thus, all the ionization observables are determined by properties of the Floquet state and can be calculated by general methods developed for constructing such states for atoms in electromagnetic fields [29,44]. We show below that in the case of a circularly polarized field they can alternatively be calculated using powerful techniques of stationary scattering theory.

B. Frame transformations

We seek for a transformation which would enable us to (i) reduce Eq. (1) to a stationary Schrödinger equation defining the Floquet state (7) and (ii) explicitly formulate the outgoing-wave boundary conditions with the outgoing flux decomposed into decoupled ionization channels. Both these requirements are essential for casting the problem in the framework of stationary scattering theory. We emphasize the second requirement, which is the key of the present approach. Its role can be illustrated by the following. It is well known that one can eliminate time from the Hamiltonian in Eq. (1) by transforming this equation to the reference frame rotating with the field [52,53]. Let us introduce an operator $\hat{R}(\alpha)$ which transforms the Cartesian components of any vector $\mathbf{r} = (x, y, z)$ under the rotation of the reference frame by an angle α about the z axis, namely, $\hat{R}(\alpha)\mathbf{r} = (x\cos\alpha + y\sin\alpha, -x\sin\alpha + y\cos\alpha, z)$. In particular, we have $\hat{R}(\omega t)\mathbf{F}(t) = \mathbf{F}(0) = (F, 0, 0)$. The electron coordinate relative to the rotating (R) frame is

$$\mathbf{r}_{\rm R} = \hat{R}(\omega t)\mathbf{r}_{\rm L}. \tag{8}$$

Substituting this and

$$\psi_{\rm L}(\mathbf{r}_{\rm L}, t) = \psi_{\rm R}(\mathbf{r}_{\rm R}, t) \tag{9}$$

into Eq. (1), one obtains the TDSE in the R frame,

$$i\frac{\partial\psi_{\rm R}(\mathbf{r}_{\rm R}, t)}{\partial t} = \left[-\frac{1}{2}\Delta_{\rm R} - \omega\hat{l}_{z_{\rm R}} + V(\mathbf{r}_{\rm R}) + Fx_{\rm R}\right]\psi_{\rm R}(\mathbf{r}_{\rm R}, t), \tag{10}$$

where $\hat{l}_{z_{\rm R}} = -i\partial/\partial\varphi_{\rm R}$. This equation was used, e.g., in early studies of ionization by a circularly polarized field from zero-range [54] and Coulomb [57,58] potentials. It can be reduced to a stationary Schrödinger equation, which complies with the first of the above requirements. However, the second requirement is not fulfilled. Indeed, the operators $\omega\hat{l}_{z_{\rm R}}$ and $Fx_{\rm R}$ do not commute with each other. Meanwhile, neither of them can be neglected in the asymptotic region $r_{\rm R} \to \infty$. Thus, eigenstates of the Hamiltonian in Eq. (10), whatever coordinates are used to construct them, cannot be expanded in decoupled channels in the asymptotic region, which greatly complicates the extraction of the ionization observables. The same applies to a similar equation obtained from the original TDSE in the velocity gauge [55,56]. This is what we call the problem of asymptotic couplings.

The transformation we need proceeds in two steps. We first transform Eq. (1) to the KH frame [45,46]. Let us introduce a reference electron trajectory in the field (3) with the velocity $\mathbf{v}(t)$ and coordinate $\mathbf{r}(t)$ satisfying

$$\dot{\mathbf{v}}(t) = -\mathbf{F}(t), \quad \dot{\mathbf{r}}(t) = \mathbf{v}(t), \tag{11}$$

and given in the L frame by

$$\mathbf{v}(t) = v_0(-\sin\omega t, \cos\omega t, 0), \quad v_0 = F/\omega, \tag{12a}$$

$$\mathbf{r}(t) = r_0(\cos\omega t, \sin\omega t, 0), \quad r_0 = F/\omega^2. \tag{12b}$$

The electron coordinate relative to the KH frame is

$$\mathbf{r}_{\rm KH} = \mathbf{r}_{\rm L} - \mathbf{r}(t). \tag{13}$$

Substituting this and

$$\psi_{\rm L}(\mathbf{r}_{\rm L}, t) = \exp\left[i\mathbf{v}(t)\mathbf{r}_{\rm KH} - \frac{iv_0^2 t}{2}\right]\psi_{\rm KH}(\mathbf{r}_{\rm KH}, t) \tag{14}$$

into Eq. (1) leads to the TDSE in the KH frame,

$$i\frac{\psi_{\rm KH}(\mathbf{r}_{\rm KH}, t)}{\partial t} = \left[-\frac{1}{2}\Delta_{\rm KH} + V[\mathbf{r}_{\rm KH} + \mathbf{r}(t)]\right]\psi_{\rm KH}(\mathbf{r}_{\rm KH}, t). \tag{15}$$

This form of the TDSE in the circular polarization case was used, e.g., in Refs. [47–51]. We now transform this equation to a rotating KH (RKH) frame. The electron coordinate relative to the RKH frame is

$$\mathbf{r}_{\rm RKH} = \hat{R}(\omega t)\mathbf{r}_{\rm KH}. \tag{16}$$

Substituting this and

$$\psi_{\rm KH}(\mathbf{r}_{\rm KH}, t) = \psi_{\rm RKH}(\mathbf{r}_{\rm RKH}, t) \tag{17}$$

into Eq. (15), we obtain the TDSE in the RKH frame,

$$i\frac{\psi_{\rm RKH}(\mathbf{r}_{\rm RKH}, t)}{\partial t} = \left[-\frac{1}{2}\Delta_{\rm RKH} - \omega\hat{l}_{z_{\rm RKH}} + V(\mathbf{r}_{\rm RKH} + \mathbf{r}_0)\right]\psi_{\rm RKH}(\mathbf{r}_{\rm RKH}, t), \tag{18}$$

where $\hat{l}_{z_{\rm RKH}} = -i\partial/\partial\varphi_{\rm RKH}$ and $\mathbf{r}_0 = (r_0, 0, 0)$. The Hamiltonian in this equation does not depend on time. Furthermore, taking into account Eq. (2), it allows separation of variables in spherical coordinates at $r_{\rm RKH} \to \infty$. Thus, both of the above requirements are fulfilled.

C. Siegert states

In this section we work in the RKH frame and, for brevity, omit the subscript of the electron coordinate. Equation (18) has solutions of the form

$$\psi_{\rm RKH}(\mathbf{r}, t) = e^{-iEt}\phi(\mathbf{r}). \tag{19}$$

Substituting this into Eq. (18), we obtain the stationary Schrödinger equation we sought

$$\left[-\frac{1}{2}\Delta - \omega\hat{l}_z + V(\mathbf{r} + \mathbf{r}_0) - E\right]\phi(\mathbf{r}) = 0. \tag{20}$$

We are interested in the solutions to this equation satisfying regularity and outgoing-wave boundary conditions formulated below. Such solutions are called atomic SSs in a rotating electric field.

To solve Eq. (20), we employ an approach which is inspired by the Born-Oppenheimer treatment of diatomic molecules [60] and was used in studies of bound states, resonances, and scattering processes in few-body Coulomb systems [61–68], vibrational spectra and chemical reactions in few-atomic systems [69–75], universalities in few-body physics [76], atomic [31] and molecular [32,33] SSs in a static electric field, etc. The Hamiltonian in Eq. (20) allows adiabatic separation of the radial r and angular $\Omega = (\theta, \varphi)$ variables in spherical coordinates. Let us rewrite Eq. (20) as

$$\left[-\frac{1}{2}\frac{\partial^2}{\partial r^2} + \hat{\mathcal{U}}(r) - E\right] r\phi(\mathbf{r}) = 0, \tag{21}$$

where

$$\hat{\mathcal{U}}(r) = \frac{\hat{\mathbf{l}}^2}{2r^2} - \omega \hat{l}_z + V(\mathbf{r} + \mathbf{r}_0). \tag{22}$$

This operator called the adiabatic Hamiltonian acts on the angular variables Ω and depends on r as a parameter. It is Hermitian and has a purely discrete spectrum of eigenstates defined by

$$\hat{\mathcal{U}}(r)\Phi_\nu(\Omega; r) = U_\nu(r)\Phi_\nu(\Omega; r), \tag{23}$$

where ν enumerates the solutions. The eigenstates also depend on r as a parameter. The eigenvalues $U_\nu(r)$ called the adiabatic potentials are real. The eigenfunctions called the adiabatic channel functions are normalized by

$$\langle \Phi_\nu(\Omega; r) | \Phi_\mu(\Omega; r) \rangle \equiv \int \Phi^*_\nu(\Omega; r)\Phi_\mu(\Omega; r)\, d\Omega = \delta_{\nu\mu}, \tag{24}$$

where $d\Omega = \sin\theta\, d\theta\, d\varphi$, and form the adiabatic basis. The solution to Eq. (21) as a function of Ω can be expanded in this basis:

$$\phi(\mathbf{r}) = r^{-1} \sum_\nu f_\nu(r)\Phi_\nu(\Omega; r). \tag{25}$$

Substituting this expansion into Eq. (21), one obtains a set of coupled ordinary differential equations defining the radial functions $f_\nu(r)$,

$$\left[-\frac{1}{2}\frac{d^2}{dr^2} + U_\nu(r) - E\right] f_\nu(r) - \sum_\mu \left[P_{\nu\mu}(r)\frac{d}{dr} + \frac{1}{2}Q_{\nu\mu}(r)\right] f_\mu(\eta) = 0, \tag{26}$$

where

$$P_{\nu\mu}(r) = \left\langle \Phi_\nu(\Omega; r) \middle| \frac{\partial \Phi_\mu(\Omega; r)}{\partial r} \right\rangle, \tag{27a}$$

$$Q_{\nu\mu}(r) = \left\langle \Phi_\nu(\Omega; r) \middle| \frac{\partial^2 \Phi_\mu(\Omega; r)}{\partial r^2} \right\rangle \tag{27b}$$

are matrices of nonadiabatic couplings. In this approach, many aspects of the dynamics of the system can be qualitatively understood already from the behavior of the adiabatic potentials [33,61–64,66,67,70,71,76]. At the same time, this approach can be very efficiently implemented in scattering calculations [71] by means of the slow variable discretization method [65] in combination with the R-matrix propagation technique [77].

Let us discuss the boundary conditions for Eqs. (26). At $r \to 0$, the potential in Eq. (22) can be expanded as

$$V(\mathbf{r} + \mathbf{r}_0)|_{r\to 0} = V(\mathbf{r}_0) + \mathbf{r}\nabla V(\mathbf{r}_0) + O(r^2). \tag{28}$$

We have assumed here that the potential is not singular at the origin in the RKH frame, which is the case for $F > 0$ even if it has a Coulomb singularity at the origin in the L frame. The second term in Eq. (28) can be treated as a perturbation. The adiabatic potentials and channel functions have the form

$$U_\nu(r)|_{r\to 0} = \frac{l(l+1)}{2r^2} - m\omega + V(\mathbf{r}_0) + O(r^2), \tag{29a}$$

$$\Phi_\nu(\Omega; r)|_{r\to 0} = Y_{lm}(\Omega) + O(r^1), \tag{29b}$$

and are thus enumerated by $\nu = (l, m)$. It can be shown that Eqs. (26) become decoupled at $r \to 0$ and the regular solutions satisfy

$$f_\nu(r)|_{r\to 0} \propto r^{l+1}. \tag{30}$$

In the opposite limit, at $r \to \infty$, we obtain from Eq. (2)

$$V(\mathbf{r}+\mathbf{r}_0)|_{r\to\infty} = -\frac{Z}{r} + \frac{Zr_0 \sin\theta\, \cos\varphi - D\cos\theta}{r^2} + O(r^{-3}). \tag{31}$$

The second term here can be treated as a perturbation. The adiabatic potentials and channel functions are given by

$$U_\nu(r)|_{r\to\infty} = -m\omega - \frac{Z}{r} + \frac{l(l+1)}{2r^2} + O(r^{-3}), \tag{32a}$$

$$\Phi_\nu(\Omega; r)|_{r\to\infty} = Y_{lm}(\Omega) + O(r^{-2}), \tag{32b}$$

and are also enumerated by $\nu = (l, m)$. We assume that this enumeration applies continuously at sufficiently large r (this implies a diabatization of the adiabatic basis discussed in Sec. III A). Then, Eqs. (26) become decoupled at $r \to \infty$ and the outgoing-wave solutions satisfy

$$f_\nu(r)|_{r\to\infty} = f_{lm} e_{lm}(k_m r), \tag{33}$$

where f_{lm} is a constant coefficient, the function $e_{lm}(z)$ defined by

$$\left[\frac{d^2}{dz^2} - \frac{l(l+1)}{z^2} + \frac{2Z/k_m}{z} + 1\right] e_{lm}(z) = 0, \tag{34a}$$

$$e_{lm}(z \to \infty) = k_m^{-1/2} z^{iZ/k_m} e^{iz}, \tag{34b}$$

gives the asymptotic form of the outgoing wave in channel (l, m), and

$$k_m = \sqrt{2(E + m\omega)}. \tag{35}$$

The branch of the square-root function meant here is defined by a branch cut made along the negative imaginary semiaxis, thus,

$$\mathrm{Re}k_m > 0 \quad \text{if} \quad \mathrm{Re}E + m\omega > 0, \tag{36a}$$

$$\mathrm{Im}k_m > 0 \quad \text{if} \quad \mathrm{Re}E + m\omega < 0. \tag{36b}$$

Conditions (36a) correspond to open channels. In this case, the function $e_{lm}(k_m r)$ in Eq. (33) indeed represents an outgoing

wave and the coefficient in Eq. (34b) is chosen such that for real E the flux in this wave is equal to unity. Conditions (36b) correspond to closed channels. In this case, the function $e_{lm}(k_m r)$ exponentially decays as r grows. Substituting Eqs. (32b), (33), and $Y_{lm}(\Omega) = e^{im\varphi}\Theta_{lm}(\theta)$ into Eq. (25) gives

$$\phi(\mathbf{r})|_{r\to\infty} = r^{-1}\sum_{lm} f_{lm}Y_{lm}(\Omega)e_{lm}(k_m r) \tag{37a}$$

$$= r^{-1}\sum_{m=-\infty}^{\infty} e^{im\varphi} f_m(\theta)e_{lm}(k_m r), \tag{37b}$$

where

$$f_m(\theta) = \sum_{l=|m|}^{\infty} f_{lm}\Theta_{lm}(\theta). \tag{38}$$

This is the form of the outgoing-wave boundary conditions for Eq. (20) we wished to obtain. The outgoing flux in Eq. (37a) is explicitly decomposed into decoupled ionization channels labeled by (l, m).

Equations (26) supplemented by the regularity (30) and outgoing-wave (33) boundary conditions constitute an eigenvalue problem. The SSs are the solutions to this problem. For $F = 0$, the Hamiltonian in Eq. (20) reduces to that in Eq. (4) plus an additional term $-\omega\hat{l}_z$. Since bound states of the field-free atom are eigenfunctions of this term, each bound state turns into an SS as the field is turned on. Note that the opposite is not true: the set of SSs is infinite and may contain states which do not have counterparts in the absence of the field, as is the case for atomic SSs in a static electric field [78]. We are interested in the SS satisfying

$$E|_{F\to 0} = E_0 - m_0\omega, \quad \phi(\mathbf{r})|_{F\to 0} = \phi_0(\mathbf{r}), \tag{39}$$

where E_0, m_0, and $\phi_0(\mathbf{r})$ characterize the unperturbed bound state defined by Eqs. (4)–(6). This bound state can also be constructed using the approach discussed above. For $F > 0$, the SS eigenvalue E becomes complex. Presented in the form

$$E = \mathcal{E} - \tfrac{i}{2}\Gamma \tag{40}$$

it defines the energy $\mathcal{E}$ and ionization rate Γ of the state. The SS eigenfunction $\phi(\mathbf{r})$ is normalized by

$$\int \phi(r, \theta, -\varphi)\phi(r, \theta, \varphi)\, d\mathbf{r} = 1. \tag{41}$$

This normalization condition is derived in Appendix A. The potential in Eq. (22) is even with respect to the reflection $y \to -y$, so the phase of the adiabatic channel functions can be chosen in such a way that

$$\Phi_\nu^*(\theta, \varphi; r) = \Phi_\nu(\theta, -\varphi; r). \tag{42}$$

We adopt this phase convention. For consistency of Eqs. (29b) and (32b) with Eq. (42), we adopt the Condon-Shortley phase convention for spherical harmonics $Y_{lm}^*(\theta, \varphi) = Y_{lm}(\theta, -\varphi)$ [79]. Then, substituting expansion (25) into Eq. (41) and using Eq. (24), we can rewrite the normalization condition as

$$\sum_\nu \int_0^\infty f_\nu^2(r)\, dr = 1. \tag{43}$$

For $F = 0$, the radial functions $f_\nu(r)$ are real and Eqs. (41) and (43) comply with Eq. (6). For $F > 0$, they become complex; note, however, that there is no complex conjugation in Eq. (43).

From Eqs. (20) and (40), acting as in the derivation of the continuity equation, we obtain

$$\Gamma|\phi(\mathbf{r})|^2 = \nabla\mathbf{j}(\mathbf{r}), \tag{44}$$

where

$$\mathbf{j}(\mathbf{r}) = \frac{-i}{2}[\phi^*(\mathbf{r})\nabla\phi(\mathbf{r}) - \phi(\mathbf{r})\nabla\phi^*(\mathbf{r})] - \omega r\,\sin\theta|\phi(\mathbf{r})|^2\mathbf{e}_\varphi \tag{45}$$

is the probability flux density in the state $\phi(\mathbf{r})$ in the RKH frame and $\mathbf{e}_\varphi = -\sin\varphi\,\mathbf{e}_x + \cos\varphi\,\mathbf{e}_y$ is a unit vector in the direction of increasing φ. Note that Eq. (45) differs from the usual expression for flux in the L frame by the second term which originates from the term $-\omega\hat{l}_z$ in Eq. (20). This term describes rotation of the probability density $|\phi(\mathbf{r})|^2$ as a solid body about the z axis in the RKH frame clockwise in its (x, y) plane, which compensates the counterclockwise rotation of the RKH frame. For $F \to 0$, the imaginary part of $f_\nu(r)$ is small and can be neglected on the left-hand side of Eq. (44) (but not on its right-hand side). Integrating both sides of the equation and using Eqs. (42) and (41), we obtain

$$\Gamma|_{F\to 0} = \int_S \mathbf{n}\mathbf{j}(\mathbf{r})\, dS\Big|_{r\to\infty}, \tag{46}$$

where $\mathbf{n} = \mathbf{r}/r$, S is a sphere of radius r, and $dS = r^2 d\Omega$. Substituting here Eq. (37a) gives

$$\Gamma|_{F\to 0} = \sum_{m=m_{\min}}^{\infty}\sum_{l=|m|}^{\infty}\Gamma_{lm} = \sum_{m=m_{\min}}^{\infty}\Gamma_m, \tag{47}$$

where

$$\Gamma_{lm} = |f_{lm}|^2, \quad \Gamma_m = \sum_{l=|m|}^{\infty}\Gamma_{lm}, \tag{48}$$

and $m_{\min}$ is the lowest m satisfying the condition (36a). These equations clarify the physical meaning of the coefficient f_{lm} as the partial ionization amplitude in channel (l, m). Equations (48) should be considered as the definitions of partial ionization rates Γ_{lm} and Γ_m in channel (l, m) and all channels with the same m, respectively, while the first equality in Eq. (47) holds only in the weak-field limit and signifies that in this limit the sum of all partial rates coincides with the total ionization rate Γ defined by Eq. (40).

The eigenvalue E and the ionization amplitudes f_{lm} extracted from the eigenfunction $\phi(\mathbf{r})$ are the main properties of the SS needed for applications. These properties for given potential $V(\mathbf{r})$, frequency ω, and field strength F should be found by solving Eq. (20).

D. Observables

Having defined the SS satisfying Eqs. (39), we now show that the ionization observables in the problem formulated in Sec. II A can be expressed in terms of the properties of this state. To find the observables, we need to return to the L frame. The state which in the RKH frame has the form (19) in the KH frame is given by (we restore subscripts of the electron

coordinate)

$$\psi_{\rm KH}(\mathbf{r}_{\rm KH},t)=e^{-iEt}\phi(\hat{R}(\omega t)\mathbf{r}_{\rm KH}) \tag{49}$$

and in the L frame by

$$\psi_{\rm L}(\mathbf{r}_{\rm L},t)=\exp\left[i\mathbf{v}(t)\mathbf{r}_{\rm L}-\frac{iv_0^2t}{2}-iEt\right]\phi(\hat{R}(\omega t)\mathbf{r}_{\rm L}-\mathbf{r}_0). \tag{50}$$

Comparing this with Eq. (7), we find

$$E_{\rm L}=E+U_p+M\omega,\quad U_p=\frac{v_0^2}{2}, \tag{51a}$$

$$\Phi(\mathbf{r}_{\rm L},t)=e^{i\mathbf{v}(t)\mathbf{r}_{\rm L}+iM\omega t}\phi(\hat{R}(\omega t)\mathbf{r}_{\rm L}-\mathbf{r}_0), \tag{51b}$$

where $M=0,\pm1,\ldots$. The terms involving M in Eqs. (51) reflect the well-known nonuniqueness [80] of the eigenvalue and eigenfunction characterizing the same Floquet state (7). Note that there is no such an ambiguity for the SS (19). By setting $M=m_0$, we select the particular $E_{\rm L}$ and $\Phi(\mathbf{r}_{\rm L},t)$ which converge to E_0 and $\phi_0(\mathbf{r}_{\rm L})$ at $F\to0$, respectively [see Eq. (39)]. In this case, the difference between ${\rm Re}E_{\rm L}$ and E_0 for $F>0$ gives the Stark shift in the L frame. Note that the difference is a sum of the Stark shift in the RKH frame ${\rm Re}E-E_0+m_0\omega$ and the ponderomotive energy U_p which compensates the Stark shift of the continuum threshold [56] in the RKH frame. Since ${\rm Im}E_{\rm L}={\rm Im}E$, the total ionization rate in the L frame coincides with that in the RKH frame and is equal to Γ.

We now turn to the PEMD. It should be noted that Floquet states in a purely monochromatic field are not observable in the exact sense of the word, and the same applies to the SSs introduced in the preceding section. However, under a certain approximation, these states define an observable PEMD. Let us consider a finite circularly polarized pulse in which the field amplitude is adiabatically turned on during the time interval $-\Delta T<t<0$, stays constant at $0<t<T$, and then is adiabatically turned off at $T<t<\Delta T$. We assume that the pulse duration T tends to infinity, which is specified by the first of the conditions

$$T\gg\max(\Delta T,2\pi/\omega),\quad \Gamma T\ll1, \tag{52}$$

and, at the same time, the second condition holds. These conditions can be satisfied simultaneously only for sufficiently weak fields F, and hence small ionization rates Γ, which is the approximation mentioned above. The same approximation is meant in the first equality in Eq. (47). Under these conditions, we can introduce the probability of ionization per unit time $p(\mathbf{k})d\mathbf{k}$ into states with photoelectron momentum $\mathbf{k}$ in the interval $d\mathbf{k}$, where the differential ionization rate $p(\mathbf{k})$ referred to in the following as the PEMD is defined by

$$p(\mathbf{k})=\frac{1}{T}|I(\mathbf{k})|^2\Big|_{T\to\infty}. \tag{53}$$

Here $I(\mathbf{k})$ is the ionization amplitude for the pulse described above given by

$$I(\mathbf{k})=-i\int_{-\infty}^{\infty}dt\int e^{-i\mathcal{S}(\mathbf{r}_{\rm L},t;\mathbf{k})}V(\mathbf{r}_{\rm L})\psi_{\rm L}(\mathbf{r}_{\rm L},t)d\mathbf{r}_{\rm L}, \tag{54}$$

where

$$\mathcal{S}(\mathbf{r}_{\rm L},t;\mathbf{k})=[\mathbf{k}+\mathbf{v}(t)][\mathbf{r}_{\rm L}-\mathbf{r}(t)]-\tfrac{1}{2}\big(\mathbf{k}^2+v_0^2\big)t \tag{55}$$

and $\psi_{\rm L}(\mathbf{r}_{\rm L},t)$ is the corresponding solution to Eq. (1) which at $t=-\Delta T$ coincides with the initial bound state (5). Equation (54) was derived for finite-range potentials in Ref. [14]; we show in Appendix B that it remains applicable for finding the PEMD for potentials with a Coulomb tail. We use this equation to express $p(\mathbf{k})$ in terms of the properties of the SS satisfying Eqs. (39). Let us first transform the spatial integral in Eq. (54) to the KH frame

$$I(\mathbf{k})=-i\int_{-\infty}^{\infty}dt\int e^{-i\mathbf{k}\mathbf{r}_{\rm KH}+i\mathbf{k}^2t/2}\times V[\mathbf{r}_{\rm KH}+\mathbf{r}(t)]\psi_{\rm KH}(\mathbf{r}_{\rm KH},t)d\mathbf{r}_{\rm KH}. \tag{56}$$

Using Eq. (15) and integrating by parts, we obtain

$$I(\mathbf{k})=\frac{-i}{2}\int_{-\infty}^{\infty}dt\int_{S_{\rm KH}}e^{-i\mathbf{k}\mathbf{r}_{\rm KH}+i\mathbf{k}^2t/2}\mathbf{n}_{\rm KH}\times[\nabla_{\rm KH}+i\mathbf{k}]\psi_{\rm KH}(\mathbf{r}_{\rm KH},t)dS_{\rm KH}|_{r_{\rm KH}\to\infty}. \tag{57}$$

Here $\mathbf{n}_{\rm KH}=\mathbf{r}_{\rm KH}/r_{\rm KH}$, $S_{\rm KH}$ is a sphere of radius $r_{\rm KH}$, and $dS_{\rm KH}=r_{\rm KH}^2d\Omega_{\rm KH}$. Taking into account Eq. (53), we are interested only in the part of the ionization amplitude which diverges as $T\to\infty$. To find this part, the integration over time in Eq. (57) can be restricted to the interval $0<t<T$. Then the function $\psi_{\rm KH}(\mathbf{r}_{\rm KH},t)$ in the integrand can be substituted from Eq. (49). Using Eq. (37b) and $\varphi_{\rm RKH}=\varphi_{\rm KH}-\omega t$, we find

$$\psi_{\rm KH}(\mathbf{r}_{\rm KH},t)|_{r_{\rm KH}\to\infty}=e^{-iEt}\sum_{m=-\infty}^{\infty}e^{im(\varphi_{\rm KH}-\omega t)}f_m(\theta_{\rm KH})e_{lm}(k_mr_{\rm KH}). \tag{58}$$

The integration over $S_{\rm KH}$ in Eq. (57) is performed using the relation

$$\int e^{-i\mathbf{k}\mathbf{r}}A(\mathbf{n})d\Omega|_{r\to\infty}=\frac{2i\pi}{kr}[e^{-ikr}A(\mathbf{n}_k)-e^{ikr}A(-\mathbf{n}_k)], \tag{59}$$

where $\mathbf{n}=\mathbf{r}/r$, $\mathbf{n}_k=\mathbf{k}/k$, and $A(\mathbf{n})$ is a smooth function of $\mathbf{n}$. Substituting the result into Eq. (53) and integrating over time using

$$\frac{1}{T}\int_0^Te^{iEt}dt\int_0^Te^{-iE't'}dt'|_{T\to\infty}=2\pi\delta(E),\quad E=E' \tag{60a}$$

$$=0,\quad E\neq E' \tag{60b}$$

we finally obtain

$$p(\mathbf{k})=\frac{(2\pi)^3}{k^2}\sum_{m=m_{\rm min}}^{\infty}\delta(k-k_m)p_m(\theta_k), \tag{61}$$

where

$$p_m(\theta_k)=|f_m(\theta_k)|^2, \tag{62}$$

and $\Omega_k=(\theta_k,\varphi_k)$ are spherical angles defining the direction of $\mathbf{k}$ in the L frame. Note that the PEMD (61) does not depend on φ_k, i.e., is axially symmetric about the k_z axis. Let us emphasize that Eq. (61) holds only in the limit $F\to0$ implied in the derivation. On the other hand, Eq. (62) should

be considered as the definition of $p_m(\theta_k)$ for any F, similar to Eqs. (48). Using Eqs. (38) and (48), we find

$$\int p_m(\theta_k) d\Omega_k = \Gamma_m. \tag{63}$$

Taking into account the δ function in Eq. (61), this relation indicates that in the weak-field limit Γ_m has the meaning of the rate of m-photon ionization. Using Eq. (47), we find

$$\int p(\mathbf{k}) \frac{d\mathbf{k}}{(2\pi)^3} = \Gamma|_{F\to 0}, \tag{64}$$

that is, in the same approximation, integrating the PEMD over the photoelectron momentum yields the total ionization rate, as expected. Thus, all the observables are expressed in terms of the SS eigenvalue E and partial ionization amplitudes f_{lm}.

III. ILLUSTRATIVE CALCULATIONS AND DISCUSSION

To illustrate the theory, we present calculations for a spherically symmetric finite-range potential

$$V(r_\mathrm{L}) = -V_0 e^{-r_\mathrm{L}^2}. \tag{65}$$

More realistic potentials with a Coulomb tail will be treated elsewhere. This potential satisfies Eq. (2) with $Z = D = 0$. We set $V_0 = 3.339\,223\,921\,5$, then it supports only one bound state with zero angular momentum and energy $E_0 = -0.5$. This state has the form (5) with $\phi_0(r_\mathrm{L}, \theta_\mathrm{L})$ independent of θ_L and $m_0 = 0$. We consider the SS originating from this state as the field F is turned on. To construct the SS, we solve Eq. (20) using the adiabatic expansion (25) implemented in a numerical procedure described in Appendix C. In this procedure, the solution to Eq. (20) for a given frequency ω is obtained starting from the unperturbed bound state for $F = 0$ and incrementing the field strength by small steps in such a way that at each step the solution changes very little, which is a numerical implementation of the analytic continuation in F. We present illustrative results for two frequencies, $\omega = 0.1$ and 0.3, both being smaller than the field-free ionization potential $|E_0|$, so that one-photon ionization is not possible. For each of the frequencies, we consider three representative values of F, namely, $F = 0.01$, 0.03, and 0.1 for $\omega = 0.1$ and $F = 0.03$, 0.1, and 0.3 for $\omega = 0.3$. In both cases, the Keldysh parameter $\gamma = \varkappa\omega/F$ decreases from 10 to 1 as F grows, where $\varkappa = \sqrt{2|E_0|}$. At least for the lower frequency, this signifies a transition from perturbative (multiphoton) to the onset of adiabatic (tunneling) ionization regime. Below we discuss basic quantities of the theory defining the SS and the ionization observables. As in Sec. II C, in this section we omit the subscript of the electron coordinate $\mathbf{r}_\mathrm{RKH}$ in the RKH frame.

A. Adiabatic potentials

We begin with the adiabatic potentials defined by Eq. (23). In the present model the potential in Eq. (22) is even with respect to the reflection $z \to -z$, and hence the adiabatic states are either even or odd functions of z. The SS originating from the ground state in the potential (65) is an even function of z. For this SS, only even adiabatic states are present in the expansion (25). We therefore discuss adiabatic potentials only for even states.

The behavior of these potentials as functions of r is illustrated in Figs. 1 and 2. At $r \to 0$, all potentials diverge $\propto r^{-2}$ [see Eq. (29a)], except the lowest one (shown by the blue line) for which $l = 0$. The adiabatic potential curves cannot cross; the degeneracy of the eigenvalues of the adiabatic Hamiltonian (22) would mean that it possesses some continuous symmetry, which is generally not the case for $F > 0$. As r grows, each potential passes through an infinite number of avoided crossings. Some of the avoided crossings are sufficiently broad and can be resolved in the figures, however, most of them are very sharp and look like real crossings. Being smoothly continued through such "crossings," *adiabatic* potentials turn into *diabatic* potentials. To highlight this behavior, the three lowest adiabatic potentials are shown by colored (blue, green, and orange) lines. The nonadiabatic couplings (27) are localized near avoided crossings. The motion in r described by Eqs. (26) through broad avoided crossings proceeds adiabatically, that is, without a change of the adiabatic state. Through sharp avoided crossings it proceeds diabatically, that is, a nonadiabatic transition between the two adiabatic states avoiding crossing occurs with probability close to unity. All these features are well known from the theory of nonadiabatic transitions (see, e.g., Refs. [81,82]) and are common to other physical systems studied by the method of adiabatic expansion in different coordinates [31–33,60–64,66,67,69–71].

At $r \to \infty$, the nonspherical part of the potential in Eq. (22) vanishes [see Eq. (31)]. As a result, all avoided crossings become very sharp and the diabatic states become decoupled. The diabatic potentials and channel functions in this limit are given by Eqs. (32a) and (32b), respectively. These states define the ionization channels in which the outgoing flux in Eq. (37a) is decomposed. They are labeled by $\nu = (l, m)$. Note that these quantum numbers are conserved along diabatic potentials, but change abruptly at avoided crossings along adiabatic potentials, which explains the need of switching from the adiabatic to the diabatic basis. As r grows, each diabatic potential converges to a constant $-m\omega$ giving the threshold energy for the corresponding channel [see Eq. (35)]. The threshold energies depend only on $m = 0, \pm 1, \ldots$ and are degenerate in $l = |m|, |m| + 1, \ldots$. Thus, from the viewpoint of scattering theory, there are infinitely many equidistant infinitely degenerate thresholds in the present problem.

As can be seen from Figs. 1 and 2, at large r the density of adiabatic states peaks along a family of smooth lines in the (r, U) plane. This feature can be understood using Eq. (32a). Consider a subset of diabatic potentials with l and m related by $l + m = n$, where $n = 0, 1, 2, \ldots$ is fixed. Substituting $m = -l + n$ into Eq. (32a) and differentiating in l, we find a minimum at $l = \omega r^2 - 1/2$ given by

$$U_n^\mathrm{env}(r) = -\frac{\omega^2 r^2}{2} + \left(n + \frac{1}{2}\right)\omega - \frac{1}{8r^2}. \tag{66}$$

This envelope function bounds the subset of potentials from below. Each potential curve from the subset touches the corresponding envelope before converging to its threshold at $r \to \infty$. For channel functions which are even in z the sum

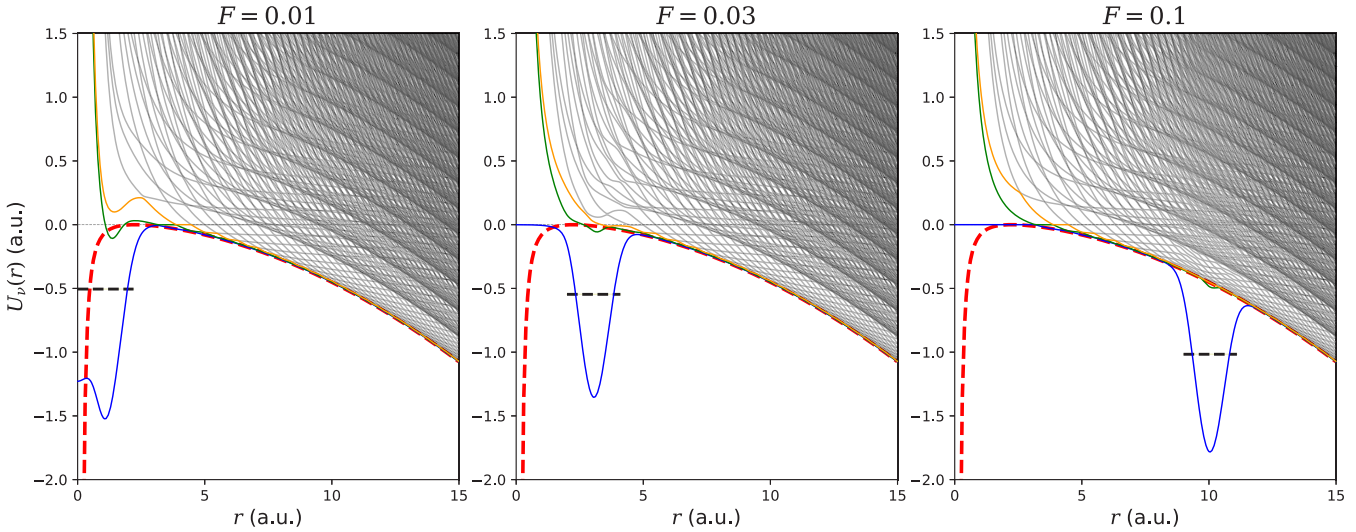

FIG. 1. Adiabatic potentials defined by Eq. (23) for $\omega = 0.1$ at three representative field strengths indicated in the figure. $r_0 = 1$, 3, and 10 for the three values of F, respectively. The three lowest potentials are shown by solid colored (blue, green, and orange) lines, the higher potentials are shown by solid gray lines. The dashed (red) line shows the lowest envelope function defined by Eq. (66) with $n = 0$. The horizontal dashed (black) line shows the real part $\mathcal{E}$ of the SS eigenvalue (40).

$l + m$ is even, so there are only subsets with $n = 0, 2, 4, \ldots$. The envelopes for these subsets are seen as the lines along which the density of adiabatic states peaks. The lowest of them with $n = 0$ is shown by the thick dashed (red) line.

The origin of the L frame, where the potential (65) is centered, in the RKH frame is located at $\mathbf{r} = -\mathbf{r}_0 = -(r_0, 0, 0)$ [see Eq. (20)], where $r_0 = F/\omega^2$. The presence of the potential well is reflected in the behavior of the adiabatic potentials near $r = r_0$. In particular, the lowest adiabatic potential forms a well in this region. At $F = 0$, this well is centered at $r = 0$. As the field F grows for a fixed ω, r_0 grows, and the well moves to the right. This potential well supports the bound part of the SS we are interested in. The real part of the SS eigenvalue (40) is shown by the horizontal dashed (black) line superimposed on the potential. Note that the well slides down along the lowest envelope (66) as F grows, remaining below the envelope. Thus, the variation of $\mathcal{E}$ with F can be approximately described by two effects: a shift of the well and a shift of the energy level in the well. The former shift can be estimated by substituting $r = r_0$ into the first term in Eq. (66), which gives $-U_p$. This shift is compensated by the ponderomotive term in Eq. (51a). The latter shift amounts to the Stark shift in the L frame. The decay of the SS proceeds in two steps involving different mechanisms. At the first step, tunneling to the right through a barrier in the lowest adiabatic potential occurs. As F grows, the potential barrier becomes lower and eventually disappears; in this case over-the-barrier ionization occurs at the first step. At the second step, the outgoing flux is distributed among the different open channels as it propagates to the asymptotic region, and the final distribution is determined by nonadiabatic couplings at numerous avoided crossings encountered on the way. Thus, the behavior

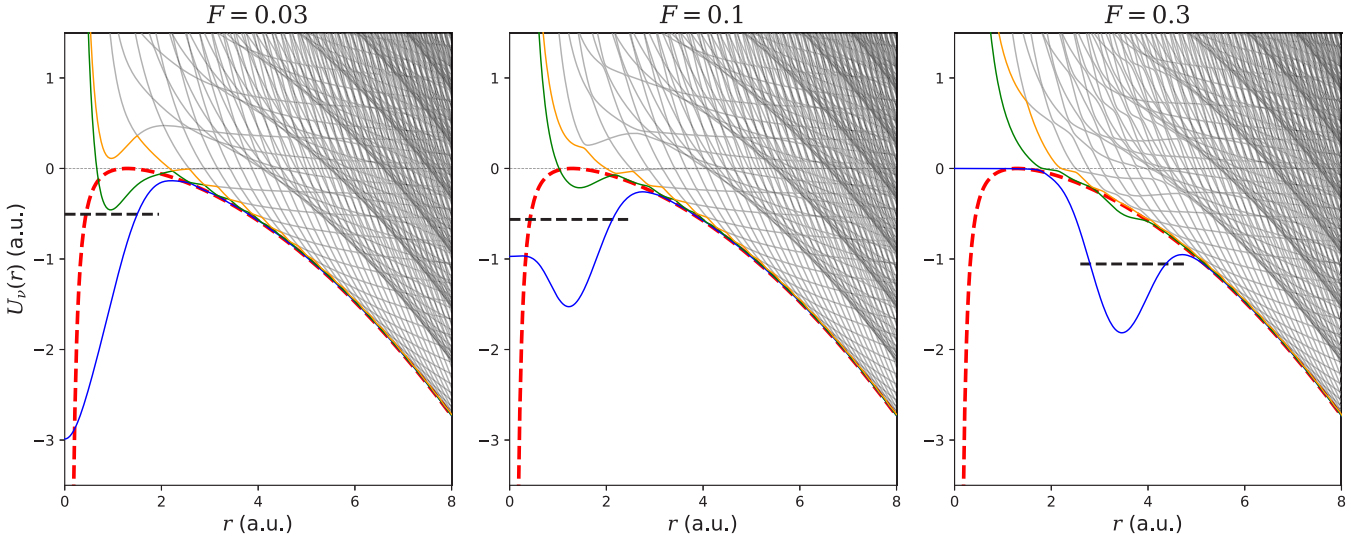

FIG. 2. Similar to Fig. 1, but for $\omega = 0.3$. In this case $r_0 \approx 0.333$, 1.11, and 3.33 for the three values of F, respectively.

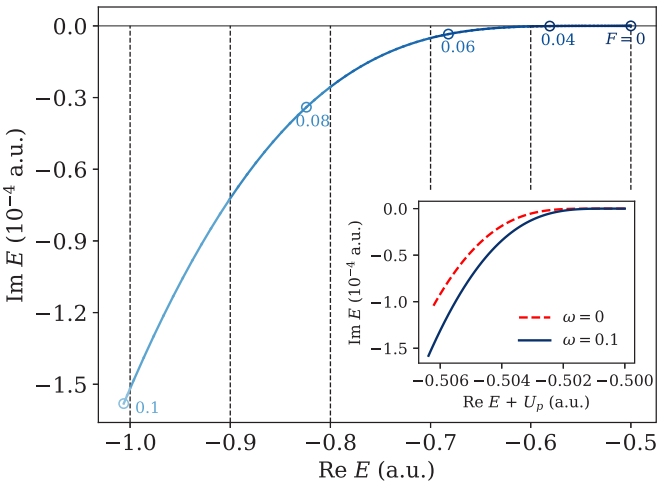

FIG. 3. Trajectory traced by the energy eigenvalue E of the dominant SS as F grows from 0 to 0.1 at $\omega = 0.1$. Some selected values of F are indicated by the circles. The vertical dashed lines show branch cuts beginning at the threshold energies $-m\omega$. The color of the line showing the trajectory changes to a lighter nuance each time the trajectory jumps to another branch of E crossing a branch cut. The inset shows a comparison of $E_{\rm L}$ obtained from Eq. (51a) (solid black line) with the energy eigenvalue of the corresponding SS in a static electric field [31] (dashed red line) in the same interval of F.

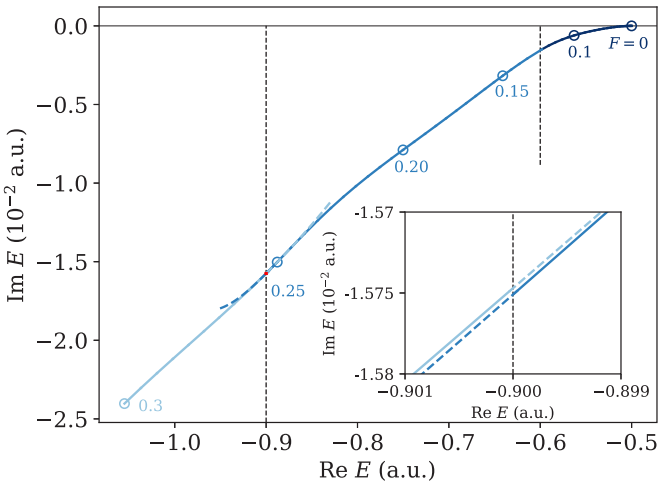

FIG. 4. Similar to Fig. 3, but for F growing from 0 to 0.3 at $\omega = 0.3$. The inset is a closeup of a tiny region shown by the red square near the point where the trajectory crosses the branch cut beginning at $E = -0.9$.

of the adiabatic potentials indeed suggests a qualitative picture explaining the very existence of the SS and the dynamics of its decay.

B. Energy eigenvalue

We next discuss the SS energy eigenvalue E. We consider it at a fixed frequency ω as a function of the field strength F. Equation (20) supplemented by regularity and outgoing-wave boundary conditions defines E as a multivalued analytic function of F. In view of Eq. (51a), the structure of the Riemann surface of this function coincides with that of the Floquet eigenvalue in a circularly polarized field [83,84]. We are interested in the branch of this function satisfying the first of Eqs. (39). As F varies, E moves along a trajectory in the complex energy plane. This trajectory is illustrated in Figs. 3 and 4. Let us follow it starting from $E = E_0$ at $F = 0$. As F begins to grow, the eigenvalue shifts to the left (the energy $\mathcal{E}$ of the SS shown by the horizontal dashed line in Figs. 1 and 2 shifts downwards) and acquires a negative imaginary part defining the ionization rate Γ of the state [see Eq. (40)]. The vertical dashed lines show the branch cuts beginning at the threshold energies $-m\omega$ and made according to the rule formulated below Eq. (35). At a certain value of F the trajectory encounters the first branch cut. To the left of this cut the corresponding channel becomes closed. The analytic continuation of E further in F along the same sheet of the Riemann surface gives k_m for this channel with the sign of Imk_m opposite to that required in Eq. (36b). The SS analytically continued through a branch cut is said to become a shadow state [85,86]. To fulfill the conditions (36), the trajectory must jump at the cut to another branch of E represented by another sheet of the Riemann surface. This situation is repeated as the trajectory encounters the second branch cut, etc. The SS which is analytically continued in F between the branch cuts, but discontinuously jumps to another sheet at the cuts in such a way that the conditions (36) remain fulfilled is called the dominant state [18]. The trajectory traced by the eigenvalue of the dominant state is shown in the figures. For both frequencies considered, this trajectory looks like a smooth continuous line, but it is not. To emphasize the fact that it is discontinuous at the branch cuts, the color of the line showing the trajectory is changed to a lighter nuance each time it crosses a cut.

The jumps of the eigenvalue E of the dominant SS at the branch cuts depend on ω and become smaller as ω decreases. Thus, for $\omega = 0.1$ and 0.3 the jumps occur in the seventh and fourth significant digit of E, respectively. The behavior of E discussed above, including a jump, is illustrated in more detail in the inset of Fig. 4. Here, a tiny region near the point where the trajectory crosses the second (counting to the left from $E = E_0$) branch cut indicated by the red square is zoomed in. The darker solid line shows the eigenvalue of the dominant SS approaching the cut as F grows. Being analytically continued in F to the left of the cut, this SS becomes a shadow state; its eigenvalue is shown by the darker dashed line. The eigenvalue of the dominant SS to the left of the cut is shown by the lighter solid line. Being analytically continued in F to the right of the cut, this SS turns into another shadow state; its eigenvalue is shown by the lighter dashed line. The dashed lines start to deviate more and more from the solid lines as they are continued further. The trajectory of the dominant eigenvalue jumps from the darker to the lighter solid line as it crosses the cut. A similar discontinuity of the trajectory occurs at each branch cut.

In the limit $\omega \to 0$, the jumps disappear and the trajectory becomes continuous. In this case, the Floquet eigenvalue $E_{\rm L}$ given by Eq. (51a) with $M = 0$ coincides with the energy eigenvalue of the corresponding SS in a static electric field [31]. The trajectories of the two eigenvalues are compared in the inset of Fig. 3. Note that the ponderomotive energy in

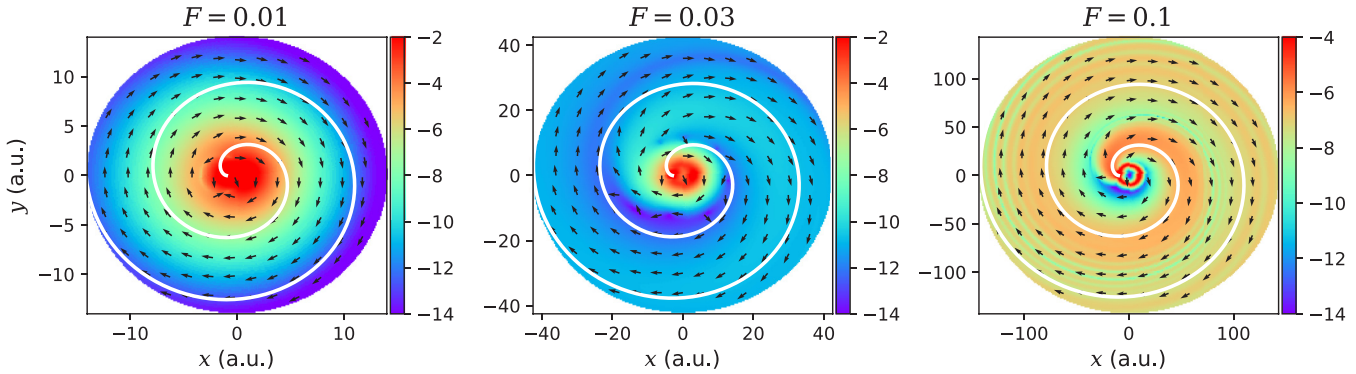

FIG. 5. Maps of the flux (45) in the (x, y) plane of the RKH frame for $\omega = 0.1$ at three field strengths F indicated in the figure. Color shows (on a base 10 logarithmic scale) the magnitude of $\mathbf{j}(\mathbf{r})$ while arrows indicate its local direction. The white line shows a classical trajectory defined by Eq. (67) which describes the motion of an electron after tunneling in the adiabatic regime.

Eq. (51a) compensates the major part of the variation of ReE with F, so that Re$E_{\rm L}$ varies in a much narrower interval. The results for $\omega = 0.1$ are seen to be not very far from the results for a static field. Note that the ionization rate at the same field in the static case is smaller.

C. Flux

We next discuss the structure of the probability flux density (45) defined by the SS eigenfunction. The map of the flux $\mathbf{j}(\mathbf{r})$ in the (x, y) plane is illustrated in Figs. 5 and 6. The distribution of its magnitude is shown by color, the arrows indicate its local direction. At weak fields, the distribution of $|\mathbf{j}(\mathbf{r})|$ is localized in the region of localization of the unperturbed bound state seen as the bright (red) spot at the center of the left panels in the figures. This region is centered at $\mathbf{r} = -\mathbf{r}_0$, and hence is slightly shifted to the left from the origin. Its radius can be estimated as $r \sim r_t$, where $r_t \approx 1.38$ is the radial turning point for the unperturbed bound state defined by $V(r_t) = E_0$. Outside this region, the flux isotropically decays as r grows in the plane. At stronger fields, the relative weight of the central maximum in the distribution of $|\mathbf{j}(\mathbf{r})|$ becomes smaller and there appears a ridge at larger r having the shape of an unwinding spiral. The arrows show that, independently of the value of F, the flux outside the central region circulates about the origin clockwise and has only a small outgoing component directed radially from the origin. Let us discuss these features in more detail.

Some of them can be understood using Eq. (45) and the asymptotic form (37a) of the SS eigenfunction. Regarding Eq. (37a), it should be noted that this equation applies at $r > r_0 + a$, where $a \sim 1$ is the radius of the potential (65); this condition is satisfied outside the central bright spot in the figures. Furthermore, the asymptotic momenta (35) for open channels have negative imaginary parts since Im$E < 0$ [see Eq. (40)]. Thus, the radial functions $e_{lm}(k_m r)$ for open channels in Eq. (37a) exponentially grow at $r \to \infty$. However, for the present values of ω and F the imaginary parts of k_m are rather small, so this growth does not reveal itself in the region shown in the figures and we do not take it into account in the discussion.

We first analyze what follows from Eqs. (45) and (37a) for the distribution of the direction of the flux. Consider the two terms in Eq. (45) separately. The first term has both radial and circular components parallel to the local unit vectors $\mathbf{e}_r = \mathbf{r}/r$ and $\mathbf{e}_\varphi$ and originating from the differentiation of Eq. (37a) in r and φ, respectively. The radial component is directed outwards and decays $\propto r^{-2}$ as r grows; it defines the outgoing flux. The circular component is directed counterclockwise since $m > 0$ for open channels in Eq. (37a), and decays $\propto r^{-3}$. The second term has only a circular component, and hence does not contribute to the outgoing flux. This term circulates

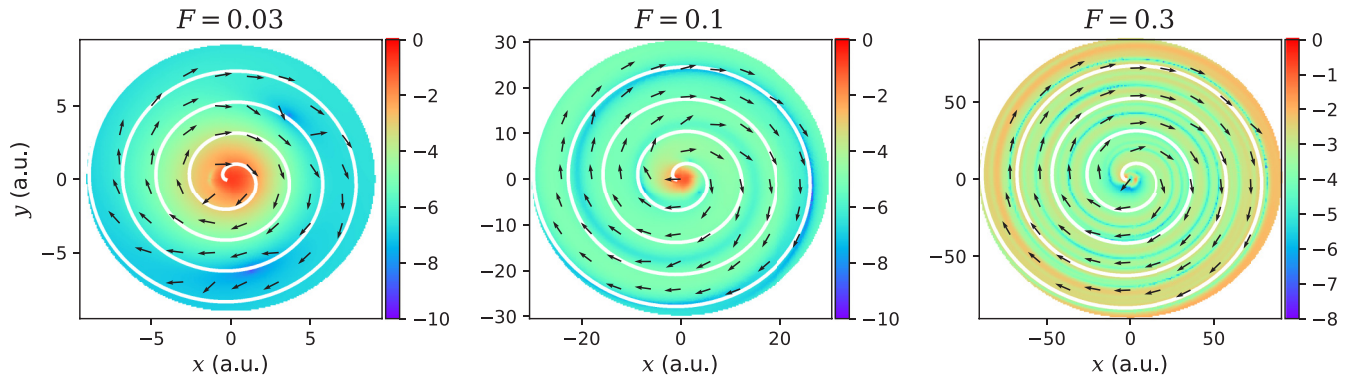

FIG. 6. Similar to Fig. 5, but for $\omega = 0.3$.

clockwise and decays $\propto r^{-1}$. Thus, the second term in Eq. (45) dominates at sufficiently large r, which explains the almost circular clockwise direction of the arrows in Figs. 5 and 6.

Let us turn to the distribution of $|\mathbf{j}(\mathbf{r})|$. At weak fields, the ionization amplitudes f_{lm} in Eq. (37a) rapidly decay as $m \geqslant m_{\min}$ and $l \geqslant m$ grow, where $m_{\min} > 0$ is the smallest m satisfying the condition (36a). In this case, the dominant contribution to the flux comes from one open channel with $l = m = m_{\min}$. If only this channel is retained in Eq. (37a), then the radial component of the first term in Eq. (45) and the second term giving the dominant contribution to the circular component of the total flux do not depend on φ, which explains the isotropy of the distributions shown in the left panels of the figures. As F grows, $|f_{lm}|$ as a function of l and m attains its maximum still at $l = m$, but this maximum is shifted to larger $m = m_{\rm ad} > m_{\min}$ (see below and the next subsection). In this case, many open channels with l and m near the maximum give comparable contributions to the flux, and Eqs. (45) and (37a) become less transparent, unless the dependence of f_{lm} on l and m is known analytically.

To understand the origin of the spiral ridge emerging in the distribution of $|\mathbf{j}(\mathbf{r})|$ at stronger fields, let us discuss this distribution in the adiabatic regime, that is, for $\omega \to 0$ and $F = O(\omega^0)$ [14]. We temporarily return to the L frame at time $t = 0$, when the x and y axes of the RKH frame are parallel to the corresponding axes of the L frame. In the adiabatic regime, the release of an electron from the parent atom at $t = 0$ occurs by tunneling in a static electric field $\mathbf{F}(0)$ equal to the instantaneous value of the rotating field (3). The exact quantum dynamics of the electron after tunneling can be described in terms of its classical motion in the field (3) [87]. The characteristic spatial extent and velocity of classical trajectories in the adiabatic regime are much larger than the size of the atom and the velocity the electron may have after tunneling [14]. Thus, only trajectories close to the one which starts at the origin with zero initial velocity are involved in the description. For the present field (3), this trajectory in the L frame is given by $\mathbf{r}(t) - \mathbf{r}(0) - \mathbf{v}(0)t$, where $\mathbf{v}(t)$ and $\mathbf{r}(t)$ are the velocity and coordinate for the reference trajectory defined by Eqs. (12). In the RKH frame, this trajectory lies in the (x, y) plane and is described by

$$x(t) = -r_0 \cos \omega t - v_0 t \sin \omega t, \tag{67a}$$

$$y(t) = -v_0 t \cos \omega t + r_0 \sin \omega t. \tag{67b}$$

This trajectory is shown by the white spiral line in Figs. 5 and 6. It does not correlate with any feature in the distributions of $|\mathbf{j}(\mathbf{r})|$ at weak fields shown in the left panels of the figures. However, it follows the spiral ridge in the right panels. This indicates that the situation at stronger fields becomes closer to the adiabatic regime and explains the origin of the ridge. Without going into further details, we mention that the distribution of $|\mathbf{j}(\mathbf{r})|$ across the ridge is determined by the transverse momentum distribution of tunneled electrons [31]. This distribution does not depend on time in the momentum domain, but spreads with time in the spatial domain. Because of the spreading, at sufficiently large t along the trajectory (67) adjacent turns of the spiral ridge begin to overlap, which results in an interference substructure seen in the right panels of the figures.

Having confirmed that in the adiabatic regime the ridge is described by the trajectory (67), we can evaluate the value of $m = m_{\rm ad}$ where $|f_{mm}|$ attains its maximum. Indeed, at large r, retaining in Eq. (37a) only one term with $l = m = m_{\rm ad}$ and substituting it into Eqs. (45), we obtain $\mathbf{e}_r \mathbf{j}(\mathbf{r})/|\phi(\mathbf{r})|^2 \approx k_{m_{\rm ad}}$. On the other hand, at large t the radial velocity for the trajectory (67) is $\dot{r}(t) \approx v_0$, where $r(t) = \sqrt{x^2(t) + y^2(t)}$. Thus, we should have $k_{m_{\rm ad}} \approx v_0$. In the adiabatic regime $E_{\rm L} = O(\omega^0)$, $v_0 = O(\omega^{-1})$, and $U_p = O(\omega^{-2})$, hence, $E = -U_p + O(\omega^0)$. From this we obtain $m_{\rm ad} \approx 2U_p/\omega = O(\omega^{-3})$. Note that in this case $m_{\min} \approx U_p/\omega \approx m_{\rm ad}/2$. Let us recall that these estimates hold asymptotically in the limit $\omega \to 0$, when, in particular, $U_p \gg E_{\rm L} \sim E_0$, which is not quite the case for the present field parameters.

D. Partial ionization rates

We next discuss partial ionization rates defined by Eqs. (48). The distribution of the values of Γ_{lm} in the (m, l) plane is illustrated by colored circles in the bottom panels of Figs. 7 and 8, while black circles in the top panels show the dependence of Γ_m on m. In the present model, f_{lm} and hence Γ_{lm} have nonzero values only for even $l - m$, therefore, for a given m in the bottom panels l takes values $m, m + 2, \ldots$. The rates Γ_{lm} decay as $l \geqslant m$ grows for a given m. At weaker fields they decay faster, so that the dominant contribution to Γ_m comes from Γ_{mm}. At stronger fields they decay slower, so that several Γ_{lm} with l close to m contribute comparably to Γ_m. At weaker fields, the rate Γ_m monotonically decays as m grows starting from $m_{\min}$. But at stronger fields it has a maximum at some $m > m_{\min}$; the position of this maximum in the adiabatic regime was estimated in the end of the preceding subsection.

According to Eq. (47), in the weak-field limit the sum of Γ_m should coincide with the total ionization rate Γ. We have confirmed this limiting behavior. In fact, the ratio of the sum of Γ_m to Γ even for the strongest fields considered here differs from unity only in the sixth and third decimal places for $\omega = 0.1$ and 0.3, respectively, so the first equality in Eq. (47) holds rather well. We note that the total rate Γ is obtained from the SS eigenvalue (40), while partial rates Γ_{lm} and Γ_m are obtained from the ionization amplitudes f_{lm} defined by the asymptotic behavior of the SS eigenfunction (37a). Equation (40) defines Γ in terms of the imaginary part of a complex number, and hence does not allow one to compute sufficiently small total rates because of the finite precision of numerical arithmetics. In particular, we could not obtain converged value of $\Gamma \sim 10^{-14}$ for $\omega = 0.1$ at $F = 0.01$. This is a common problem of calculating small ionization rates by methods relying on Eq. (40) [88]. Meanwhile, f_{lm} is obtained by matching the inner and outer solutions (see Appendix C), which enables one to compute almost arbitrarily small partial rates Γ_{lm} limited only by the smallest number that a computer can treat. Thus, we have accurately calculated partial rates in a huge range of their values, as shown in the figures. Using these rates and Eq. (47) we obtain $\Gamma \approx 1.876 \times 10^{-14}$ for $\omega = 0.1$ at $F = 0.01$, which overcomes the numerical limitation of Eq. (40). The results shown in Figs. 7 and 8 demonstrate the computational power of the present approach.

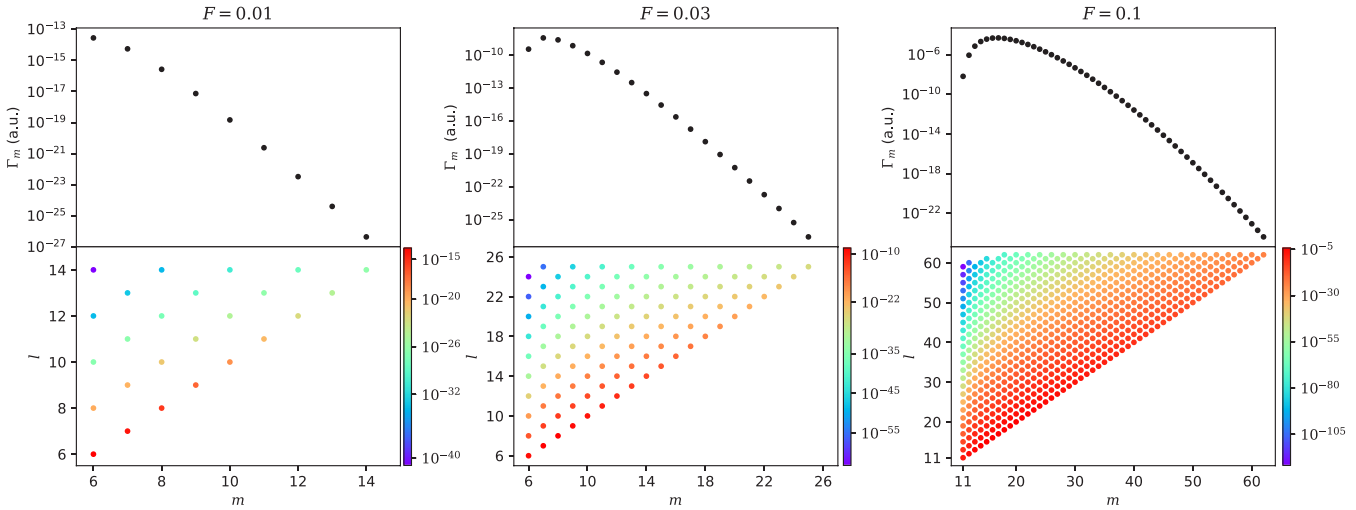

FIG. 7. Partial ionization rates Γ_m as a function of m (top panels) and Γ_{lm} as a function of m and l (bottom panels) for $\omega = 0.1$ at three field strengths indicated in the figure. Color of the circles in the bottom panels shows (on a logarithmic scale) the value of Γ_{lm}. $m_{\min} = 6$, 6, and 11 for the three values of F, respectively.

E. Photoelectron momentum distribution

We finally discuss the PEMD defined by Eq. (61). Because of the δ functions in Eq. (61), it is more convenient to consider the angular distributions $p_m(\theta_k)$ of photoelectrons which have absorbed m photons defined by Eqs. (38) and (62). These distributions are illustrated in Figs. 9 and 10. The values of $p_m(\theta_k)$ as a function of m and θ_k are shown by color along arcs of radius $k = \mathrm{Re}k_m = \mathrm{Re}\sqrt{m\omega + E}$, where E is the corresponding SS eigenvalue, in the plane with coordinates $k_\rho = \sqrt{k_x^2 + k_y^2} = k \sin\theta_k$ and $k_z = k\cos\theta_k$. Functions $p_m(\theta_k)$ do not change under the transformation $\theta_k \to \pi - \theta_k$ because only terms with even $l - m$ are present in Eq. (38), so we show only the $k_z > 0$ half-plane. For a given m, the distributions $p_m(\theta_k)$ monotonically decay as θ_k decreases from $\pi/2$ ($k_z = 0$) to 0 ($k_\rho = 0$). Their dependence on m at $\theta_k = \pi/2$ resembles that of Γ_m shown in the top panels of Figs. 7 and 8, which is expectable taking into account Eq. (63).

It can be seen that the set of the distributions $p_m(\theta_k)$ considered as functions of k_ρ and k_z has a smooth envelope. The maximum of the envelope lies on the k_ρ axis and shifts to larger k_ρ as F grows. Simultaneously, the envelope becomes symmetric about its maximum and takes a bell-like shape (if the $k_z < 0$ half-plane is included). To understand these features, we again consider the situation in the adiabatic regime. In the limit $\omega \to 0$ and $F = O(\omega^0)$, at sufficiently weak fields, the PEMD (61) properly averaged over k (see below) is given by [14,89,90]

$$p(\mathbf{k}) = \text{const} \times \exp\left[-\frac{(k_\rho - k_{\max})^2 + k_z^2}{\sigma^2}\right], \qquad (68)$$

where $k_{\max} = v_0$, $\sigma = \sqrt{F/\varkappa}$, and the coefficient does not depend on k_ρ and k_z. The distribution (68) is localized in the photoelectron momentum space in a narrow pipe along a circle of radius $k_{\max} = O(\omega^{-1})$ lying in the (k_x, k_y) plane and has a Gaussian shape in a section across the circle with the width

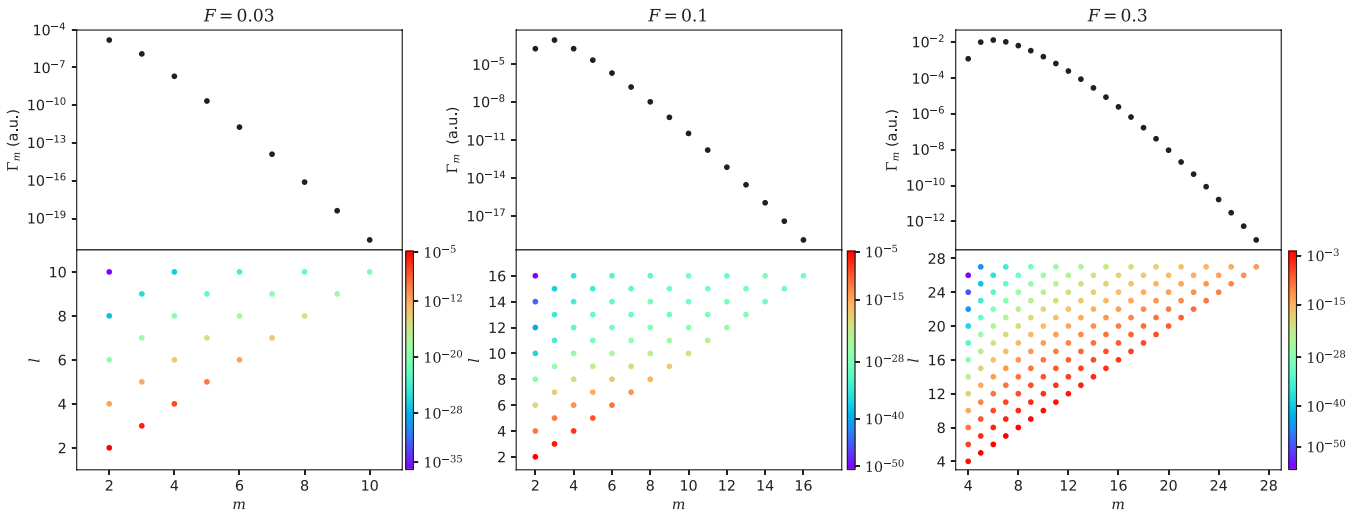

FIG. 8. Similar to Fig. 7, but for $\omega = 0.3$. In this case, $m_{\min} = 2$, 2, and 4 for the three values of F, respectively.

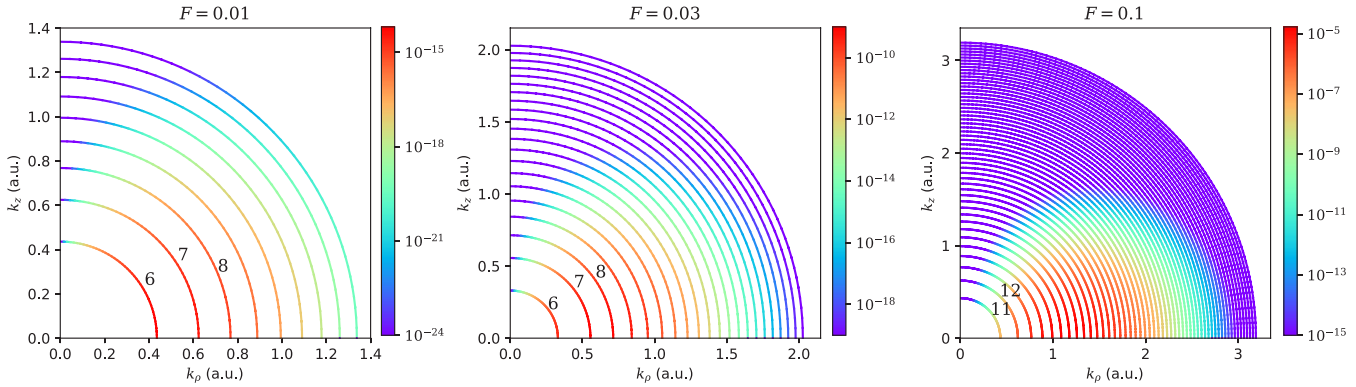

FIG. 9. Angular distributions $p_m(\theta_k)$ of photoelectrons which have absorbed m photons for $\omega = 0.1$ at three field strengths indicated in the figure. The values of $p_m(\theta_k)$ as a function of m and θ_k are shown by color (on a logarithmic scale) along arcs of radius $k = \mathrm{Re}k_m$ in the plane with coordinates $k_\rho = k\ \sin\theta_k$ and $k_z = k\ \cos\theta_k$. The numbers indicate several lowest values of m for open channels.

$\sigma = O(\omega^0)$. The continuous distribution (68) is obtained by averaging Eq. (61) over intervals of k larger than $k_{m+1} - k_m \approx \omega/v_0^2 = O(\omega^2)$ but smaller than σ in the leading order of the asymptotic expansion in ω. It was shown that in the first-order approximation this distribution preserves its shape, but the radius of the circle becomes $k_{\max} = v_0 + \varkappa^2\omega/6F$, where the second term represents a nonadiabatic correction [34]. This prediction of the adiabatic theory was validated numerically by solving the TDSE [34] and confirmed experimentally [91]. Let us compare it with the results of the present stationary calculations. To this end, we replace each $\delta(k - k_m)$ in Eq. (61) in the corresponding interval $(k_{m-1} + k_m)/2 < k < (k_m + k_{m+1})/2$ by $2/(k_{m+1} - k_{m-1})$, so that the integral over the interval remains equal to unity. The resulting stepwise distribution as a function of k_ρ and k_z is fitted by Eq. (68), where the coefficient and $k_{\max}$ are treated as fitting parameter. The thus-obtained values of $k_{\max}$ are shown in Fig. 11. The upper panel shows the results for $\omega = 0.1$ and varying F, while the lower panel shows the results for $F = 0.1$ and varying ω. The error bars represent 95% confidence levels obtained by multiplying the estimated variances from the fit with corresponding Student's t values [92]. Some of the data points at larger ω in the lower panel have larger error bars because the maximum of the distribution in this case is close to $k_\rho = 0$. The solid (black) and dashed (red) lines show the predictions of the adiabatic theory in the leading-order and first-order approximations, respectively. The first-order theory better describes the numerical results, especially for decreasing ω at a fixed F (in the bottom panel), where the adiabatic approximation holds. Thus, Eq. (68) describing the PEMD in the adiabatic regime qualitatively explains the shape of the distributions shown in Figs. 9 and 10.

IV. CONCLUSION AND OUTLOOK

We have introduced and investigated atomic SSs in a rotating electric field. These states are defined by Eq. (20) subject to regularity and outgoing-wave boundary conditions. They are related to Floquet states in a monochromatic circularly polarized field. The circular polarization case occupies a special position in the theory of Floquet states: as far as we know, only in this case the Floquet eigenvalue problem can be reduced to a single time-independent 3D equation which is free from asymptotic couplings and hence allows to explicitly formulate the outgoing-wave boundary conditions. This justifies introducing a new name for the solutions to Eq. (20). All the observables characterizing strong-field ionization in a monochromatic circularly polarized field are expressed in terms of properties of the SSs. We have proposed and demonstrated an efficient method to calculate them using powerful techniques of stationary scattering theory. The method yields not only the SS eigenvalue defining the

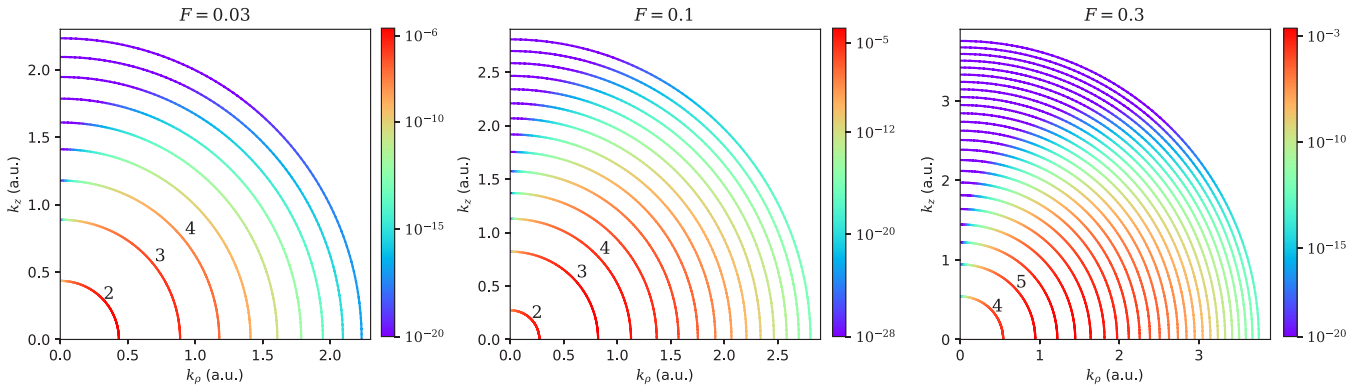

FIG. 10. Similar to Fig. 9, but for $\omega = 0.3$.

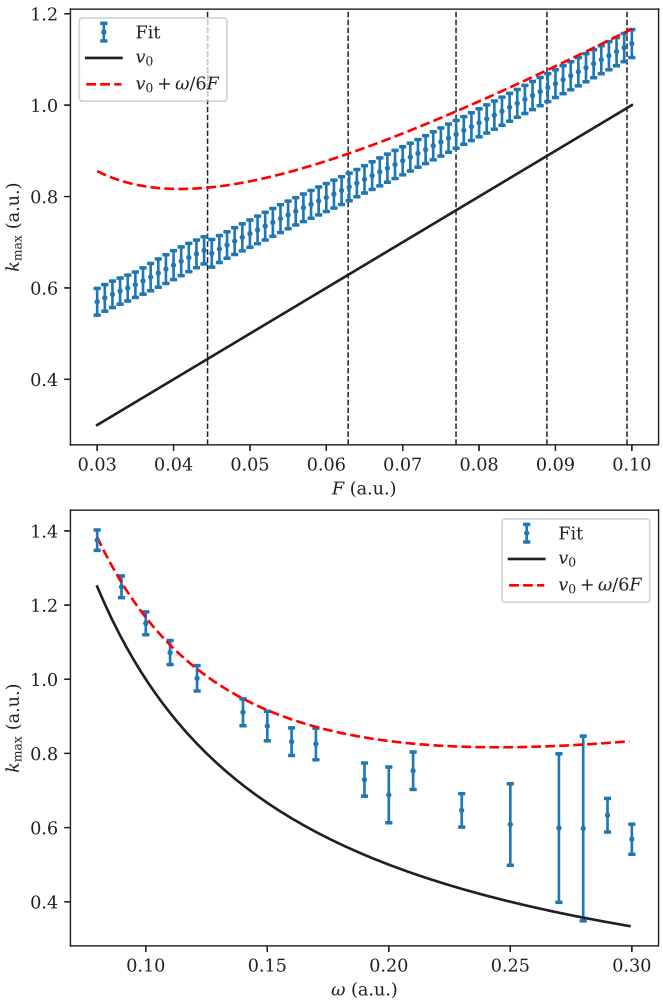

FIG. 11. The radius k_{max} of the circle in the (k_x, k_y) plane along which the PEMD (61) is localized in the adiabatic regime as a function of F at $\omega = 0.1$ (top panel) and as a function of ω at $F = 0.1$ (bottom panel). Small solid circles with error bars show the values obtained by fitting the present results for the PEMD by Eq. (68). Solid (black) and dashed (red) lines show the predictions of the adiabatic theory in the leading-order [14,89,90] and first-order (for the present system $\varkappa = 1$) [34] approximations, respectively.

Stark-shifted energy and total ionization rate of the state, but also the properly normalized SS eigenfunction defining partial ionization amplitudes and rates and the photoelectron momentum distribution. These developments turn the SSs into a useful tool for strong-field studies.

Let us mention two possible extensions of this work which are of interest for applications. First, it would be instructive to obtain the asymptotic solution to Eq. (20) in the weak-field limit. The weak-field asymptotic theory of SSs in a static electric field [90] works quantitatively for field strengths up to $F \lesssim 0.1$ [93,94], which covers many of current strong-field experiments, and was shown to be very helpful for the analysis of experiments [40,41,95–97]. Second, as mentioned in the Introduction, the SSs introduced in this work provide an essential technical element needed for developing a theory for finite circularly polarized pulses based on the asymptotic expansion in the inverse number of optical cycles in the pulse. Such a theory is needed, e.g., for investigating pulse envelope effects in strong-field observables. Its development is in progress.

ACKNOWLEDGMENTS

We thank L. O. Krainov for discussions and S. Shishido for a help in making Figs. 5 and 6. This work was supported in part by JSPS KAKENHI Grants No. 19H00887 and No. 21K03417.

APPENDIX A: NORMALIZATION CONDITION FOR THE SIEGERT STATES

SSs are generally defined as eigenstates of a Hamiltonian $\hat{H}$ which are regular at any finite point and satisfy outgoing-wave boundary conditions in the asymptotic region. In the original paper [98], Siegert introduced such states for motion with zero angular momentum in spherically symmetric potentials. Later, the concept was extended to states with nonzero angular momentum in spherically symmetric potentials [99,100], potentials without any symmetry [101], atoms [31], and molecules [32,33] in a static electric field, and in this paper we further extend it to atoms in a rotating electric field. The complete set of SSs includes ordinary bound states of the system, if they exist. For bound states, the eigenvalues are real, the eigenfunctions exponentially decay in the asymptotic region, and the normalization condition is usually presented in the form

$$\int \phi^*(\mathbf{r})\phi(\mathbf{r})\, d\mathbf{r} = 1, \tag{A1}$$

where the asterisk denotes complex conjugation. At the same time, there exist infinitely many SSs whose eigenvalues are complex and eigenfunctions exponentially grow in the asymptotic region. The normalization condition (A1) is not suitable for such SSs because the integral diverges. How to properly generalize Eq. (A1) to states with growing eigenfunctions is one of the central issues in the theory of SSs.

A general approach to the derivation of the normalization condition for SSs was proposed in Ref. [102]. Let $G(\mathbf{r}, \mathbf{r}'; E) = \langle \mathbf{r}|(\hat{H} - E - i0)^{-1}|\mathbf{r}'\rangle$ be the outgoing-wave Green's function for the Hamiltonian $\hat{H}$. The approach of Ref. [102] is based on the following two statements. First,

$$(E - \lambda)G(\mathbf{r}, \mathbf{r}'; \lambda)|_{\lambda \to E} = \phi(\mathbf{r})\bar{\phi}(\mathbf{r}'), \tag{A2}$$

where $\phi(\mathbf{r})$ is the eigenfunction of $\hat{H}$ corresponding to the eigenvalue E and $\bar{\phi}(\mathbf{r})$ is an adjoint function. Note that Eq. (A2) implies a certain normalization of $\phi(\mathbf{r})$. Second, using the Hilbert identity and Eq. (A2) it can be shown that

$$\int \bar{\phi}(\mathbf{r})\phi(\mathbf{r})\, d\mathbf{r} = 1. \tag{A3}$$

In view of this relation, the function $\phi(\mathbf{r})$ is said to be normalized to unity. To specify the normalization condition (A3) one needs to find the adjoint function $\bar{\phi}(\mathbf{r})$. This can be done by establishing a relation between $G(\mathbf{r}, \mathbf{r}'; E)$ and $G(\mathbf{r}', \mathbf{r}; E)$. For example, for all Hamiltonians considered in Refs. [31–33,98–101] the Green's function is symmetric with respect to permutation of its arguments, $G(\mathbf{r}, \mathbf{r}'; E) = G(\mathbf{r}', \mathbf{r}; E)$, and hence $\bar{\phi}(\mathbf{r}) = \phi(\mathbf{r})$, as follows from Eq. (A2).

Thus, for such Hamiltonians SSs should be normalized by Eq. (A3) without the bar. Note that in this case the asterisk in Eq. (A1) can be omitted because eigenfunctions of bound states can be chosen to be real, so Eq. (A1) reduces to Eq. (A3). For SSs with growing eigenfunctions the integral in Eq. (A3) also diverges. However, it can be regularized. Indeed, many different techniques to regularize the normalization integral yielding the same final result were proposed [31,102–107].

Let us apply the same argumentation to the Hamiltonian in Eq. (20). The potential energy term does not modify the permutation properties of the Green's function, so let us omit this term and consider the Green's function defined by

$$\left[-\frac{1}{2}\Delta - \omega\hat{l}_z - E\right]G_\omega(\mathbf{r},\mathbf{r}';E) = \delta(\mathbf{r}-\mathbf{r}'). \tag{A4}$$

The outgoing-wave solution to this equation is given by

$$G_\omega(\mathbf{r},\mathbf{r}';E) = \frac{e^{-i\pi/4}}{(2\pi)^{3/2}}\int_0^\infty \exp\left[\frac{i(r^2+r'^2-2zz')}{2t} - \frac{i\rho\rho'}{t}\cos(\varphi-\varphi'+\omega t) + iEt\right]\frac{dt}{t^{3/2}}, \tag{A5}$$

where $\rho = r\sin\theta$. This function satisfies $G_\omega(\mathbf{r}',\mathbf{r};E) = G_{-\omega}(\mathbf{r},\mathbf{r}';E)$, and hence so does the Green's function for the Hamiltonian in Eq. (20). Let E_ω and $\phi_\omega(\mathbf{r})$ denote an eigenvalue and the corresponding eigenfunction of Eq. (20) for a given ω. On the one hand, taking into account the axial symmetry of the potential in the L frame, we have $E_{-\omega} = E_\omega$ and $\phi_{-\omega}(\mathbf{r}) = \phi_\omega(r,\theta,-\varphi)$. On the other hand, using Eq. (A2), we obtain $\bar{\phi}_\omega(\mathbf{r}) = \phi_{-\omega}(\mathbf{r})$. Thus, $\bar{\phi}_\omega(\mathbf{r}) = \phi_\omega(r,\theta,-\varphi)$, which leads to the normalization condition (41). We mention that, taking into account Eq. (51b), this complies with the normalization condition for Floquet states in a circularly polarized laser field [18,108].

APPENDIX B: ON THE DEFINITION OF THE IONIZATION AMPLITUDE

In this Appendix we work in the laboratory frame and omit the subscript L. Consider Eq. (1) for a finite pulse of arbitrary polarization. We assume that $\mathbf{F}(t<t_{\rm in}) = \mathbf{F}(t>t_{\rm fin}) = 0$. Let $\psi(\mathbf{r},t)$ be the solution to Eq. (1) satisfying the initial condition $\psi(\mathbf{r},t<t_{\rm in}) = e^{-iE_0t}\phi_0(\mathbf{r})$. Let $\psi_{\mathbf{k}}^{(\pm)}(\mathbf{r}) = \langle\mathbf{r}|\mathbf{k}\pm\rangle$ denote *in* (+) and *out* (−) scattering states of the field-free atom with asymptotic momentum $\mathbf{k}$ normalized by $\langle\mathbf{k}\pm|\mathbf{k}'\pm\rangle = (2\pi)^3\delta(\mathbf{k}-\mathbf{k}')$. Then the ionization amplitude is defined by

$$A(\mathbf{k}) = \int\left[\psi_{\mathbf{k}}^{(-)}(\mathbf{r})e^{-i\mathbf{k}^2t/2}\right]^*\psi(\mathbf{r},t)d\mathbf{r}\Big|_{t>t_{\rm fin}}. \tag{B1}$$

Meanwhile, in Ref. [14], the ionization amplitude was defined by

$$I(\mathbf{k}) = \int[e^{i\mathbf{k}\mathbf{r}-i\mathbf{k}^2t/2}]^*\chi(\mathbf{r},t)d\mathbf{r}\Big|_{t\to\infty}, \tag{B2}$$

where $\chi(\mathbf{r},t) = (1-\hat{P}_b)\psi(\mathbf{r},t)$ and $\hat{P}_b$ is the projector onto the subspace of bound states of the field-free atom. In particular, the latter definition was used as the starting point in the derivation of Eq. (54). Since $I(\mathbf{k})$ is obtained by projecting on a plane wave $e^{i\mathbf{k}\mathbf{r}} = \langle\mathbf{r}|\mathbf{k}\rangle$ instead of an exact scattering state $\psi_{\mathbf{k}}^{(-)}(\mathbf{r})$, it is not clear how it is related to $A(\mathbf{k})$, especially for potentials with a Coulomb tail. Let us discuss this issue.

Let $\hat{H} = \hat{H}_0 + \hat{V}$ denote the Hamiltonian in Eq. (4), where $\hat{H}_0 = \hat{\mathbf{p}}^2/2$. We can rewrite Eq. (B1) as $A(\mathbf{k}) = \langle\mathbf{k}-|e^{i\hat{H}t}|\chi(t)\rangle|_{t>t_{\rm fin}}$. Thus,

$$|\chi(t)\rangle|_{t>t_{\rm fin}} = e^{-i\hat{H}t}\int A(\mathbf{k})|\mathbf{k}-\rangle\frac{d\mathbf{k}}{(2\pi)^3}. \tag{B3}$$

Møller's wave operators are defined by [109]

$$\hat{\Omega}_\pm = \lim_{t\to\mp\infty}\exp(i\hat{H}t)\exp[-i\hat{H}_0t - is(t,(2\hat{H}_0)^{1/2})], \tag{B4}$$

where the term with

$$s(t,k) = -\mathrm{sgn}(t)\frac{Z}{k}\ln(2k^2|t|) \tag{B5}$$

is a modification introduced by Dollard [110] accounting for the Coulomb tail of the potential [see Eq. (2)]. These operators transform plane waves into scattering states $|\mathbf{k}\pm\rangle = \hat{\Omega}_\pm|\mathbf{k}\rangle$. Rewriting Eq. (B2) as $I(\mathbf{k}) = \langle\mathbf{k}|e^{i\hat{H}_0t}|\chi(t)\rangle|_{t\to\infty}$, substituting Eq. (B3), and using Eq. (B4), we obtain

$$I(\mathbf{k}) = e^{-is(t,k)}A(\mathbf{k}). \tag{B6}$$

Thus, for finite-range potentials with $Z=0$ the amplitudes $I(\mathbf{k})$ and $A(\mathbf{k})$ coincide with each other, while for Coulomb-tail potentials with $Z\neq 0$ they differ by a time-dependent phase factor. In both cases $|I(\mathbf{k})|^2 = |A(\mathbf{k})|^2$, so the two amplitudes yield the same PEMD. We mention that the last equality was verified by numerical calculations [111].

APPENDIX C: NUMERICAL PROCEDURE

To find the SS eigenvalue E and eigenfunction $\phi(\mathbf{r})$ defining the ionization amplitudes f_{lm} for given potential, frequency, and field strength we need to solve Eq. (20) subject to the regularity and outgoing-wave boundary conditions formulated in Sec. II C. Our approach is based on the adiabatic expansion (25). However, Eqs. (26) are not convenient for implementing this expansion in numerical calculations because of the many very narrow peaks of nonadiabatic couplings (27) at avoided crossings of the adiabatic potentials (see Figs. 1 and 2). To overcome this difficulty, we implement Eq. (25) by means of the slow variable discretization (SVD) method [65] in combination with the R-matrix propagation technique [77]. This approach has proven to be very efficient in treating various scattering processes [31,32,68,71,112–117]. Here, we outline basic steps of the present numerical procedure.

Adiabatic basis. The adiabatic potentials $U_\nu(r)$ and channel functions $\Phi_\nu(\Omega;r)$ are obtained by solving Eq. (23) using an expansion in spherical harmonics $Y_{lm}(\Omega)$. The first two terms in Eq. (22) are diagonal in this basis. The matrix of the potential is calculated numerically using Gaussian quadratures in θ and φ. For potentials invariant under the reflection $z\to -z$ the solutions to Eq. (23) are either even or odd with respect to $\theta\to\pi-\theta$. In this case, only harmonics with either even or odd $l-m$ should be retained in the expansion, respectively, which reduces the size of the resulting algebraic eigenvalue problem by half. The channel functions are normalized using Eq. (24); their phase is chosen to satisfy Eq. (42).

Inner region $0 \leqslant r \leqslant r_c$. In this region, Eq. (20) is treated without any approximations. The radial axis is divided into $N_{\rm sec}$ equal sectors with boundaries at

$$0 = \bar{r}_0 < \bar{r}_1 < \cdots < \bar{r}_{N_{\rm sec}} = r_c. \tag{C1}$$

All sectors are treated similarly. Consider the kth sector

$$\bar{r}_- \equiv \bar{r}_{k-1} \leqslant r \leqslant \bar{r}_k \equiv \bar{r}_+. \tag{C2}$$

The R-matrix basis in the sector is defined by

$$\left[-\frac{1}{2}\frac{\partial}{\partial r}r^2\frac{\partial}{\partial r} + \hat{\mathcal{L}} + r^2(\hat{\mathcal{U}}(r) - \bar{E})\right]\bar{\phi}(\mathbf{r}) = 0, \tag{C3}$$

where

$$\hat{\mathcal{L}} = \frac{r^2}{2}[\delta(r-\bar{r}_+) - \delta(r-\bar{r}_-)]\frac{\partial}{\partial r} \tag{C4}$$

is the Bloch operator [118]. To construct this basis, we introduce a new variable x,

$$r(x) = s(x_c + x), \quad -1 \leqslant x \leqslant 1, \tag{C5a}$$

$$s = \frac{\bar{r}_+ - \bar{r}_-}{2}, \quad x_c = \frac{\bar{r}_+ + \bar{r}_-}{\bar{r}_+ - \bar{r}_-}. \tag{C5b}$$

Let x_i and $\pi_i(x)$, $i = 1, \ldots, N_{\rm DVR}$, be the Gauss-Legendre quadrature points and discrete variable representation (DVR) basis functions [119–122]. The solutions to Eq. (C3) are sought in the form of the SVD expansion [65]

$$\bar{\phi}(\mathbf{r}) = \sum_{i=1}^{N_{\rm DVR}}\sum_{\nu=1}^{N_{\rm ch}} c_{i\nu}\pi_i(x)\Phi_\nu(\Omega; r_i), \tag{C6}$$

where $r_i = r(x_i)$ and $N_{\rm ch}$ is the number of adiabatic channels included in the calculations. Substituting this into Eq. (C3) leads to the algebraic eigenvalue problem

$$\sum_{j=1}^{N_{\rm DVR}}\sum_{\mu=1}^{N_{\rm ch}} K_{ij}O_{i\nu,j\mu}c_{j\mu} + r_i^2[U_\nu(r_i) - \bar{E}]c_{i\nu} = 0, \tag{C7}$$

where

$$K_{ij} = \frac{1}{2}\int_{-1}^{1}\frac{d\pi_i}{dx}(x_c + x)^2\frac{d\pi_j}{dx}dx, \tag{C8a}$$

$$O_{i\nu,j\mu} = \langle\Phi_\nu(\Omega; r_i)|\Phi_\mu(\Omega; r_j)\rangle. \tag{C8b}$$

The matrix (C8a) representing the kinetic energy for the motion in r is known analytically [122]. The overlap matrix (C8b) between adiabatic channels at different quadrature points is calculated in the same way as the normalization integral in Eq. (24). Let $\bar{E}_n$ and $c^n_{i\nu}$ denote the eigenvalues and eigenvectors of Eq. (C7) and $\bar{\phi}_n(\mathbf{r})$ denote the corresponding solution to Eq. (C3), where $n = 1, \ldots, N_{\rm SVD} = N_{\rm DVR}N_{\rm ch}$. The solutions are normalized by

$$\int_{\bar{r}_-}^{\bar{r}_+} r^2 dr \int \bar{\phi}_n(r, \theta, -\varphi)\bar{\phi}_m(r, \theta, \varphi)d\Omega$$

$$= s\sum_{i=1}^{N_{\rm DVR}}\sum_{\nu=1}^{N_{\rm ch}} r_i^2 c^n_{i\nu}c^m_{i\nu} = \delta_{nm}, \tag{C9}$$

in accordance with Eq. (41).

Within the sector (C2), the solution to Eq. (20) can be expanded in the R-matrix basis,

$$\phi(\mathbf{r}) = \sum_{n=1}^{N_{\rm SVD}} C_n\bar{\phi}_n(\mathbf{r}), \tag{C10}$$

where

$$C_n = \frac{1}{2(\bar{E}_n - E)}\sum_{\nu=1}^{N_{\rm ch}}\left[\bar{f}^+_{n\nu}d_\nu(\bar{r}_+) - \bar{f}^-_{n\nu}d_\nu(\bar{r}_-)\right]. \tag{C11}$$

Here

$$\bar{f}^\pm_{n\nu} = r\langle\Phi_\nu(\Omega; r)|\bar{\phi}_n(\mathbf{r})\rangle|_{r=\bar{r}_\pm} = \bar{r}_\pm\sum_{j=1}^{N_{\rm DVR}}\sum_{\mu=1}^{N_{\rm ch}} c^n_{j\mu}\pi_j(\pm 1)O^\pm_{\nu,j\mu} \tag{C12}$$

are the coefficients in the adiabatic expansion of $\bar{\phi}_n(\mathbf{r})$ at the boundaries of the sector [compare with Eq. (25)], where

$$O^\pm_{\nu,j\mu} = \langle\Phi_\nu(\Omega; \bar{r}_\pm)|\Phi_\mu(\Omega; r_j)\rangle \tag{C13}$$

are the overlap matrices between adiabatic channels at the boundaries of the sector and quadrature points inside it, and

$$d_\nu(r) = r\left\langle\Phi_\nu(\Omega; r)\middle|\frac{\partial\phi(\mathbf{r})}{\partial r}\right\rangle. \tag{C14}$$

The surface amplitudes (C12) can be calculated using the adiabatic and R-matrix bases, which have already been constructed. The coefficients (C11) additionally involve $d_\nu(\bar{r}_\pm)$ defined by Eq. (C14) in terms of the solution (C10) itself; the way of calculating these quantities is described below. Using Eqs. (C9) and (C10), we obtain the norm of $\phi(\mathbf{r})$ within the sector

$$\mathcal{N}_k = \int_{\bar{r}_-}^{\bar{r}_+} r^2 dr \int \phi(r, \theta, -\varphi)\phi(r, \theta, \varphi)d\Omega = \sum_{n=1}^{N_{\rm SVD}} C_n^2. \tag{C15}$$

Note that there is no complex conjugation in the last expression, so $\mathcal{N}_k$ is generally complex.

Outer region $r_c \leqslant r$. In this region, couplings between adiabatic channels are neglected and the solution to Eq. (20) is assumed to be given by Eqs. (37). The radial functions in these expansions are defined by Eq. (34),

$$e_{lm}(z) = k_m^{-1/2}(-2i)^{l+1-iZ/k_m}z^{l+1}e^{iz} \times U(l+1-iZ/k_m, 2l+2, -2iz), \tag{C16}$$

where $U(a, b, z)$ is a confluent hypergeometric function [123]. For potentials satisfying Eq. (2) with $Z = 0$ these functions take the form

$$e_{lm}(z) = \sqrt{\frac{\pi z}{2k_m}}\, i^{l+1}H^{(1)}_{l+1/2}(z), \tag{C17}$$

where $H^{(1)}_\nu(z)$ is the Hankel function of the first kind [123].

Eigenvalue. The SS eigenvalue E is determined by the requirement that the solution to Eq. (20) must satisfy the regularity (30) and outgoing-wave (33) boundary conditions. This requirement can be imposed, and hence the eigenvalue found, without constructing the solution explicitly. Following Ref. [124], we introduce the R matrix $\mathbf{R}(r; E)$ defined by

$$\mathbf{f}(r) = \mathbf{R}(r; E)\mathbf{d}(r), \tag{C18}$$

where $\mathbf{f}(r)$ and $\mathbf{d}(r)$ are vectors with components $f_\nu(r)$ and $d_\nu(r)$, $\nu = 1, \ldots N_{\rm ch}$, defined by Eqs. (25) and (C14), respectively. Using Eq. (C10), we obtain

$$\mathbf{R}(\bar{r}_\pm; E) = \pm\mathcal{R}^{(\pm,\pm)} - \mathcal{R}^{(\pm,\mp)}[\mathbf{R}(\bar{r}_\mp; E) \pm \mathcal{R}^{(\mp,\mp)}]^{-1}\mathcal{R}^{(\mp,\pm)}, \tag{C19}$$

where $\mathcal{R}^{(\pm,\pm)}$ are matrices with elements

$$\mathcal{R}^{(\pm,\pm)}_{\nu\mu} = \frac{1}{2}\sum_{n=1}^{N_{\rm SVD}} \frac{\bar{f}^{\pm}_{n\nu}\bar{f}^{\pm}_{n\mu}}{\bar{E}_n - E}. \tag{C20}$$

These equations implement the R-matrix propagation technique [77] for the present problem. Using them, we can propagate the R matrix between the boundaries $\bar{r}_\pm$ of a sector, and hence through any sector in any direction. From Eq. (30) we have

$$R_{\nu\mu}(0; E) = 0. \tag{C21}$$

On the other hand, from Eq. (33) we find

$$R_{\nu\mu}(r_c; E) = R_\nu \delta_{\nu\mu},$$

$$R_{lm} = \left.\frac{e_{lm}(z)}{k_m[de_{lm}(z)/dz - e_{lm}(z)/z]}\right|_{z=k_m r_c}, \tag{C22}$$

where $\nu = (l, m)$. Let $\bar{r}_K$ be a boundary between sectors somewhere inside the interval (C1). Starting from Eq. (C21) and propagating the R matrix outwards to $\bar{r}_K$, we obtain $\mathbf{R}_{\rm left}(\bar{r}_K; E)$ characterizing solutions to Eq. (20) satisfying Eq. (30). Starting from Eq. (C22) and propagating the R matrix inwards to $\bar{r}_K$, we obtain $\mathbf{R}_{\rm right}(\bar{r}_K; E)$ characterizing solutions to Eq. (20) satisfying Eq. (33). The solution we seek must satisfy both boundary conditions. Furthermore, this solution as well as its derivative in r must be continuous at $r = \bar{r}_K$, which leads to the matching condition

$$\det[\mathbf{R}_{\rm left}(\bar{r}_K; E) - \mathbf{R}_{\rm right}(\bar{r}_K; E)] = 0. \tag{C23}$$

This equation defines the eigenvalue E. Having an initial guess for E for given potential and field parameters (see below), it can be solved iteratively using the Newton method [125].

Eigenfunction and ionization amplitudes. The eigenvector of the difference of the R matrices in Eq. (C23) corresponding to the zero eigenvalue is proportional to $\mathbf{d}(\bar{r}_K)$. The coefficient of proportionality is determined by the normalization procedure discussed below. Let us temporarily disregard the coefficient and assume that a properly normalized $\mathbf{d}(\bar{r}_K)$ is found from Eq. (C23). The vector $\mathbf{d}(r)$ can be propagated between boundaries of a sector similar to Eq. (C19),

$$\mathbf{d}(\bar{r}_\pm) = \mp[\mathbf{R}(\bar{r}_\pm; E) \mp \mathcal{R}^{(\pm,\pm)}]^{-1}\mathcal{R}^{(\pm,\mp)}\mathbf{d}(\bar{r}_\mp). \tag{C24}$$

Starting from $\mathbf{d}(\bar{r}_K)$ and using Eq. (C24), we obtain $\mathbf{d}(\bar{r}_k)$ for all $k = 0, 1, \ldots, N_{\rm sec}$. These vectors complete the information needed to construct the solution to Eq. (20) in the inner region using Eq. (C10). The last of them, $\mathbf{d}(r_c)$, defines the coefficients in Eqs. (37) giving the solution in the outer region,

$$f_{lm} = \frac{R_{lm} d_{lm}(r_c)}{e_{lm}(k_m r_c)}. \tag{C25}$$

Thus, the SS eigenfunction $\phi(\mathbf{r})$ is globally defined and the ionization amplitudes f_{lm} found.

We now recall that the normalization condition (41) has not been imposed yet. Using Eq. (C15), we obtain the norm of $\phi(\mathbf{r})$ in the inner region:

$$\mathcal{N}_{\rm in} = \sum_{k=1}^{N_{\rm sec}} \mathcal{N}_k. \tag{C26}$$

The norm in the outer region is obtained from Eq. (37a):

$$\mathcal{N}_{\rm out} = \sum_{lm}^{N_{\rm ch}} f_{lm}^2 \int_{r_c}^{\infty} e_{lm}^2(k_m r) dr. \tag{C27}$$

For $Z = 0$, the integral here can be calculated analytically. For $Z \neq 0$, it is calculated numerically by rotating the integration path into the complex r plane, so that the integrand decays as $|r|$ grows [31]. The total norm is $\mathcal{N} = \mathcal{N}_{\rm in} + \mathcal{N}_{\rm out}$. Thus, the SS eigenfunction and ionization amplitudes found above should be renormalized as $\phi(\mathbf{r}) \to \mathcal{N}^{-1/2}\phi(\mathbf{r})$ and $f_{lm} \to \mathcal{N}^{-1/2} f_{lm}$.

Numerical analytic continuation. The procedure described above requires as an input information an initial guess for the eigenvalue E. We adopt an approach in which the field frequency ω is fixed and the field strength F is incremented by small steps. We start from $F = 0$, in which case the solution to Eq. (20) is given by Eqs. (39). At each step in F, the initial guess is provided by the value of E found at the previous step. The initial set of k_m is defined by Eqs. (35) and (36) with $E = E_0 - m_0\omega$. At each Newton iteration in E, whether for the same F or after incrementing it, we choose the branch of the square-root function in Eq. (35) closest to the value of k_m at the previous iteration. If steps in F are sufficiently small, this procedure realizes a numerical implementation of the analytic continuation in F. Note that at any step in F the procedure can change the variable and continue by incrementing ω at a fixed F. Thus, the SS can be constructed as an analytic function of both F and ω.

The procedure begins at $F = 0$ with k_m satisfying Eqs. (36) and, hence, at the initial stage, analytically continues the dominant state [18]. As the eigenvalue crosses the first branch cut it encounters in the complex E plane (see Figs. 3 and 4), the corresponding channel becomes closed. However, further analytic continuation yields a wrong sign for this channel in Eq. (36b) because E has a negative imaginary part. In other words, being analytically continued across the cut, the dominant state turns into a shadow state [86]. To return to the dominant state, the procedure jumps at the cut to another sheet of the Riemann surface of E by finding a solution to Eq. (C23) in the vicinity of the current one satisfying Eqs. (36). After the jump, the solution is analytically continued until encountering the next branch cut, etc.

Practical details. We finally discuss some details regarding numerical parameters used to produce the present results. The potential (65) satisfies $|V(r > 7)| < 10^{-20}$. We set $r_c = r_0 + 7$, which ensures that Eqs. (37) hold at $r > r_c$ with high accuracy. The number of sectors $N_{\rm sec}$ in the inner region is set equal to the integer part of r_c, so that the sector length is close to 1. We use $N_{\rm DVR} = 10$ quadrature points per sector. The matching condition (C23) is applied at a sector boundary closest to $r_0 + 2$. The number of adiabatic channels $N_{\rm ch}$ needed for convergence strongly depends on the

field parameters. To accurately calculate adiabatic channels, the basis must include all spherical harmonics with $l \leqslant l_{\max}$, $|m| \leqslant l$, and even $l - m$. The largest demand in this paper is for $\omega = 0.08$ and $F = 0.1$, which required $N_{\rm ch} \approx 2400$ and $l_{\max} = 190$. To prevent the loss of numerical accuracy for such large values of l in Eqs. (C17) and (C27), we use a multiple precision package MPFUN2015 [126]. The linear algebra part of the calculations is implemented using routines from LAPACK [127]. The overall accuracy of the calculations is rather high, the relative errors of the resulting SS eigenvalue E and ionization amplitudes f_{lm} are $\sim 10^{-10}$ and $\sim 10^{-5}$, respectively.

[1] F. Krausz and M. Ivanov, Attosecond physics, Rev. Mod. Phys. **81**, 163 (2009).

[2] L. V. Keldysh, Ionization in the field of a strong electromagnetic wave, Zh. Eksp. Teor. Fiz. **47**, 1945 (1964) [Sov. Phys. JETP **20**, 1307 (1965)].

[3] F. H. M. Faisal, Multiple absorption of laser photons by atoms, J. Phys. B: At. Mol. Phys. **6**, L89 (1973).

[4] H. R. Reiss, Effect of an intense electromagnetic field on a weakly bound system, Phys. Rev. A **22**, 1786 (1980).

[5] P. B. Corkum, Plasma Perspective on Strong Field Multiphoton Ionization, Phys. Rev. Lett. **71**, 1994 (1993).

[6] P. B. Corkum and F. Krausz, Attosecond science, Nat. Phys. **3**, 381 (2007).

[7] F. H. M. Faisal and A. Becker, 'Intense-field many-body *S*-matrix theory' and mechanism of laser induced double ionization of helium, in *Selected Topics on Electron Physics*, edited by D. M. Campbell and H. Kleinpoppen (Plenum, New York, 1996), p. 397.

[8] A. Becker and F. H. M. Faisal, Intense-field many-body *S*-matrix theory, J. Phys. B: At. Mol. Opt. Phys. **38**, R1 (2005).

[9] R. Kopold, D. B. Milošević, and W. Becker, Rescattering Processes for Elliptical Polarization: A Quantum Trajectory Analysis, Phys. Rev. Lett. **84**, 3831 (2000).

[10] P. Salières, B. Carré, L. Le Déroff, F. Grasbon, G. G. Paulus, H. Walther, R. Kopold, W. Becker, D. B. Milošević, A. Sanpera, and M. Lewenstein, Feynman's path-integral approach for intense-laser-atom interactions, Science **292**, 902 (2001).

[11] W. Becker, F. Grasbon, R. Kopold, D. B. Milošević, G. G. Paulus, and H. Walther, Above-threshold ionization: From classical features to quantum effects, in *Advances in Atomic and Molecular Physics*, edited by B. Bederson and H. Walther (Academic Press, New York, 2002), Vol. 48, p. 35.

[12] M. V. Frolov, N. L. Manakov, E. A. Pronin, and A. F. Starace, Model-Independent Quantum Approach for Intense Laser Detachment of a Weakly Bound Electron, Phys. Rev. Lett. **91**, 053003 (2003).

[13] M. V. Frolov, N. L. Manakov, and A. F. Starace, Effective-range theory for an electron in a short-range potential and a laser field, Phys. Rev. A **78**, 063418 (2008).

[14] O. I. Tolstikhin and T. Morishita, Adiabatic theory of ionization by intense laser pulses: Finite-range potentials, Phys. Rev. A **86**, 043417 (2012).

[15] N. L. Manakov and A. G. Fainshtein, Decay of a weakly bound level in a monochromatic field, Zh. Eksp. Teor. Fiz. **79**, 751 (1990) [Sov. Phys. JETP **52**, 382 (1980)].

[16] N. L. Manakov, V. D. Ovsiannikov, and L. P. Rapoport, Atoms in a laser field, Phys. Rep. **141**, 320 (1986).

[17] S.-I. Chu, Recent developments in semiclassical Floquet theories for intense-field multiphoton processes, in *Advances in Atomic and Molecular Physics*, edited by D. R. Bates and B. Bederson (Academic Press, New York, 1985), Vol. 21, p. 197.

[18] R. M. Potvliege and R. Shakeshaft, Nonperturbative treatment of multiphoton ionization within the Floquet framework, in *Atoms in Intense Laser Fields*, edited by M. Gavrila (Academic Press, New York, 1992), p. 373.

[19] M. Gavrila and J. Z. Kamiński, Free-Free Transitions in Intense High-Frequency Laser Fields, Phys. Rev. Lett. **52**, 613 (1984).

[20] M. Gavrila, Atomic structure and decay in high-frequency fields, in *Atoms in Intense Laser Fields*, edited by M. Gavrila (Academic Press, New York, 1992), p. 435.

[21] M. Gavrila, Atomic stabilization in superintense laser fields, J. Phys. B: At. Mol. Opt. Phys. **35**, R147 (2002).

[22] P. G. Burke, P. Francken, and C. J. Joachain, *R*-matrix-Floquet theory of multiphoton processes, Europhys. Lett. **13**, 617 (1990).

[23] P. G. Burke, P. Francken, and C. J. Joachain, *R*-matrix-Floquet theory of multiphoton processes, J. Phys. B: At. Mol. Opt. Phys. **24**, 761 (1991).

[24] P. G. Burke, J. Colgan, D. H. Glass, and K. Higgins, *R*-matrix-Floquet theory of molecular multiphoton processes, J. Phys. B: At. Mol. Opt. Phys. **33**, 143 (2000).

[25] C. J. Joachain, *R*-matrix-Floquet theory of multiphoton processes: concepts, results and perspectives, J. Mod. Opt. **54**, 1859 (2007).

[26] T.-S. Ho and S.-I. Chu, Coupled dressed-states formalism for multiphoton excitation and population inversion by coherent pulses, Chem. Phys. Lett. **141**, 315 (1987).

[27] Y. Huang and S.-I. Chu, A stationary treatment of time-dependent Hamiltonian by the many-mode Floquet formalism and its application to the study of effects of laser pulses in multiphoton processes, Chem. Phys. Lett. **225**, 46 (1994).

[28] S.-I. Chu and D. A. Telnov, Beyond the Floquet theorem: generalized Floquet formalisms and quasienergy methods for atomic and molecular multiphoton processes in intense laser fields, Phys. Rep. **390**, 1 (2004).

[29] C. J. Joachain, N. J. Kylstra, and R. M. Potvliege, *Atoms in Intense Laser Fields* (Cambridge University Press, Cambridge, 2012).

[30] B. D. Esry, Y. Wang, D. Ursrey, H. R. Larsson, D. J. Tannor, N. Douguet, K. Bartschat, A. N. Grum-Grzhimailo, B. Schulz, A. Saenz, L. Marder, D. M. Reich, C. P. Koch, A. Scrinzi, F. Morales, T. Bredtmann, H. G. Muller, S. Patchkovskii, X. Wang, F. Robicheaux *et al.*, Comparing the performance of time-dependent-Schrödinger-equation solvers for the 800-nm, one-electron-atom, strong-field problem, in APS Division of Atomic, Molecular and Optical Physics Meeting Abstracts, APS Meeting Abstracts, Vol. 2018 (APS, Ridge, NY, 2018), p. T01.036.

[31] P. A. Batishchev, O. I. Tolstikhin, and T. Morishita, Atomic Siegert states in an electric field: Transverse momentum distribution of the ionized electrons, Phys. Rev. A **82**, 023416 (2010).

[32] L. Hamonou, T. Morishita, and O. I. Tolstikhin, Molecular Siegert states in an electric field, Phys. Rev. A **86**, 013412 (2012).

[33] V. N. T. Pham, O. I. Tolstikhin, and T. Morishita, Molecular Siegert states in an electric field. II. Transverse momentum distribution of the ionized electrons, Phys. Rev. A **89**, 033426 (2014).

[34] M. Ohmi, O. I. Tolstikhin, and T. Morishita, Analysis of a shift of the maximum of photoelectron momentum distributions generated by intense circularly polarized pulses, Phys. Rev. A **92**, 043402 (2015).

[35] Y. Zhou, O. I. Tolstikhin, and T. Morishita, Near-Forward Rescattering Photoelectron Holography in Strong-Field Ionization: Extraction of the Phase of the Scattering Amplitude, Phys. Rev. Lett. **116**, 173001 (2016).

[36] T. Morishita and O. I. Tolstikhin, Adiabatic theory of strong-field photoelectron momentum distributions near a backward rescattering caustic, Phys. Rev. A **96**, 053416 (2017).

[37] V. N. T. Pham, O. I. Tolstikhin, and T. Morishita, Images of molecular orbitals in strong-field photoelectron momentum distributions generated by circularly polarized pulses, Phys. Rev. A **99**, 013428 (2019).

[38] O. I. Tolstikhin and T. Morishita, Strong-field ionization, rescattering, and target structure imaging with vortex electrons, Phys. Rev. A **99**, 063415 (2019).

[39] H. Geiseler, N. Ishii, K. Kaneshima, F. Geier, T. Kanai, O. I. Tolstikhin, T. Morishita, and J. Itatani, Carrier-envelope phase mapping in laser-induced electron diffraction, Phys. Rev. A **94**, 033417 (2016).

[40] Y. Ito, M. Okunishi, T. Morishita, O. I. Tolstikhin, and K. Ueda, Rescattering photoelectron spectroscopy of heterodiatomic molecules with an analytical returning photoelectron wave packet, Phys. Rev. A **97**, 053411 (2018).

[41] M. Okunishi, Y. Ito, V. Sharma, S. Aktar, K. Ueda, R. R. Lucchese, A. I. Dnestryan, O. I. Tolstikhin, S. Inoue, H. Matsui, and T. Morishita, Rescattering photoelectron spectroscopy of the CO_2 molecule: Progress towards experimental discrimination between theoretical target-structure models, Phys. Rev. A **100**, 053404 (2019).

[42] T. Mizuno, N. Ishii, T. Kanai, P. Rosenberger, D. Zietlow, M. F. Kling, O. I. Tolstikhin, T. Morishita, and J. Itatani, Observation of the quantum shift of a backward rescattering caustic by carrier-envelope phase mapping, Phys. Rev. A **103**, 043121 (2021).

[43] S.-I. Chu and W. P. Reinhardt, Intense Field Multiphoton Ionization Via Complex Dressed States: Application to the H Atom, Phys. Rev. Lett. **39**, 1195 (1977).

[44] R. M. Potvliege, STRFLO: A program for time-independent calculations of multiphoton processes in one-electron atomic systems I. Quasienergy spectra and angular distributions, Comput. Phys. Commun. **114**, 42 (1998).

[45] H. A. Kramers, in *Collected Scientific Papers* (North-Holland, Amsterdam, 1956), p. 272.

[46] W. C. Henneberger, Perturbation Method for Atoms in Intense Light Beams, Phys. Rev. Lett. **21**, 838 (1968).

[47] L. Dimou and F. H. M. Faisal, New Class of Resonance in the $e + H^+$ Scattering in an Excimer Laser Field, Phys. Rev. Lett. **59**, 872 (1987).

[48] A. Giusti-Suzor and P. Zoller, Rydberg electrons in laser fields: A finite-range-interaction problem, Phys. Rev. A **36**, 5178 (1987).

[49] P. Marte and P. Zoller, Hydrogen in intense laser fields: Radiative close-coupling equations and quantum-defect parametrization, Phys. Rev. A **43**, 1512 (1991).

[50] U. Lambrecht, L. Dimou, and F. H. M. Faisal, Ab initio rates of multiphoton ionization of the isoelectronic species H, He^+, and Li^{2+} in the vuv and xuv frequency regions, Phys. Rev. A **57**, 2832 (1998).

[51] H. Miyagi and K. Someda, Unified understanding of tunneling ionization and stabilization of atomic hydrogen in circularly and linearly polarized intense laser fields, Phys. Rev. A **82**, 013402 (2010).

[52] F. V. Bunkin and A. M. Prokhorov, The excitation and ionization of atoms in a strong radiation field, Zh. Eksp. Teor. Fiz. **46**, 1090 (1964) [Sov. Phys. JETP **19**, 739 (1964)].

[53] W. Salzman, Exact semiclassical solution for the time evolution of a quantum-mechanical system in a circularly polarized monochromatic driving field, Chem. Phys. Lett. **25**, 302 (1974).

[54] N. L. Manakov and L. P. Rapoport, Particle with low binding energy in a circularly polarized field, Zh. Eksp. Teor. Fiz. **69**, 842 (1975) [Sov. Phys. JETP **42**, 430 (1975)].

[55] I. J. Berson, Multiphoton ionization and stimulated bremsstrahlung radiation in the case of short-range potentials, J. Phys. B: At. Mol. Phys. **8**, 3078 (1975).

[56] H. G. Muller, A. Tip, and M. J. van der Wiel, Ponderomotive force and AC Stark shift in multiphoton ionisation, J. Phys. B: At. Mol. Phys. **16**, L679 (1983).

[57] S.-I. Chu, Quasienergy formalism for intense field multiphoton ionization of atoms induced by circularly polarized radiation, Chem. Phys. Lett. **54**, 367 (1978).

[58] M. A. Preobrazhenskĭ and L. P. Rapoport, Quasistationary states of a hydrogen atom in the field of a strong monochromatic wave, Zh. Eksp. Teor. Fiz. **78**, 929 (1980) [Sov. Phys. JETP **51**, 468 (1980)].

[59] Y. B. Zel'dovich, The quasienergy of a quantum-mechanical system subjected to a periodic action, Zh. Eksp. Teor. Fiz. **51**, 1492 (1966) [Sov. Phys. JETP **24**, 1006 (1967)].

[60] M. Born and R. Oppenheimer, Zur quantentheorie der molekeln, Ann. Phys. **389**, 457 (1927).

[61] J. Macek, Properties of autoionizing states of He, J. Phys. B: At. Mol. Phys. **1**, 831 (1968).

[62] U. Fano, Unified treatment of collisions, Phys. Rev. A **24**, 2402 (1981).

[63] C. D. Lin, Doubly excited states, including new classification schemes, in *Advances in Atomic and Molecular Physics*, edited by D. R. Bates and B. Bederson (Academic Press, New York, 1986), Vol. 22, p. 77.

[64] C. D. Lin, Hyperspherical coordinate approach to atomic and other Coulombic three-body systems, Phys. Rep. **257**, 1 (1995).

[65] O. I. Tolstikhin, S. Watanabe, and M. Matsuzawa, 'Slow' variable discretization: a novel approach for Hamiltonians allowing adiabatic separation of variables, J. Phys. B: At. Mol. Opt. Phys. **29**, L389 (1996).

[66] T. Morishita and C. D. Lin, Comprehensive analysis of electron correlations in three-electron atoms, Phys. Rev. A **59**, 1835 (1999).

[67] O. I. Tolstikhin and M. Matsuzawa, Exploring the separability of the three-body Coulomb problem in hyperspherical elliptic coordinates, Phys. Rev. A **63**, 062705 (2001).

[68] Y. Zhou, S. Watanabe, O. I. Tolstikhin, and T. Morishita, Hyperspherical calculations of ultralow-energy collisions in Coulomb three-body systems, Phys. Rev. A **92**, 032713 (2015).

[69] A. Kuppermann and P. G. Hipes, Three-dimensional quantum mechanical reactive scattering using symmetrized hyperspherical coordinates, J. Chem. Phys. **84**, 5962 (1986).

[70] R. T. Pack and G. A. Parker, Quantum reactive scattering in three dimensions using hyperspherical (APH) coordinates. Theory, J. Chem. Phys. **87**, 3888 (1987).

[71] O. I. Tolstikhin and H. Nakamura, Hyperspherical elliptic coordinates for the theory of light atom transfer reactions in atom-diatom collisions, J. Chem. Phys. **108**, 8899 (1998).

[72] Y. Suzuki and K. Varga, Constrained correlated-Gaussians for hyperspherical calculations, Few-Body Syst. **60**, 3 (2019).

[73] H. Suno, Study of the van der Waals rare gas trimers Ne_3, Ar_3, Kr_3, and Xe_3 using hyperspherical coordinates, Few-Body Syst. **60**, 6 (2019).

[74] V. Kokoouline, D. Lapierre, A. Alijah, and V. Tyuterev, Localized and delocalized bound states of the main isotopologue $^{48}O_3$ and of ^{18}O-enriched $^{50}O_3$ isotopomers of the ozone molecule near the dissociation threshold, Phys. Chem. Chem. Phys. **22**, 15885 (2020).

[75] B. Lepetit, Computation and analysis of bound vibrational spectra of the neon tetramer using row orthonormal hyperspherical coordinates, J. Chem. Phys. **153**, 104302 (2020).

[76] C. H. Greene, P. Giannakeas, and J. Pérez-Ríos, Universal few-body physics and cluster formation, Rev. Mod. Phys. **89**, 035006 (2017).

[77] K. L. Baluja, P. G. Burke, and L. A. Morgan, *R*-matrix propagation program for solving coupled second-order differential equations, Comput. Phys. Commun. **27**, 299 (1982).

[78] A. V. Gets and O. I. Tolstikhin, Static-field-induced states, Phys. Rev. A **87**, 013419 (2013).

[79] E. U. Condon and G. H. Shortley, *The Theory of Atomic Spectra* (Cambridge University Press, Cambridge, 1964).

[80] H. Sambe, Steady states and quasienergies of a quantum-mechanical system in an oscillating field, Phys. Rev. A **7**, 2203 (1973).

[81] E. E. Nikitin and S. Y. Umanskii, *Theory of Slow Atomic Collisions* (Springer, Berlin, 1984).

[82] H. Nakamura, *Nonadiabatic Transition: Concepts, Basic Theories and Applications* (World Scientific, New Jersey, 2012).

[83] N. L. Manakov and A. G. Fainshtein, Quasistationary quasienergy states and convergence of perturbation series in a monochromatic field, Teor. Mat. Fiz. **48**, 385 (1981) [Sov. Phys. Theor. Math. Phys. **48**, 815 (1981)].

[84] M. Pont and R. Shakeshaft, Analytic structure of the ac quasienergy in the complex-field plane, Phys. Rev. A **43**, 3764 (1991).

[85] V. N. Ostrovskii, Many-photon ionization, resonance scattering on a nonstationary potential, and complex poles of the *S*-matrix, Teor. Mat. Fiz. **33**, 126 (1977) [Sov. Phys. Theor. Math. Phys. **33**, 923 (1977)].

[86] R. M. Potvliege and R. Shakeshaft, Movement and interplay of the bound state, resonance, and shadow poles of the scattering amplitude in multiphoton processes, Phys. Rev. A **38**, 6190 (1988).

[87] R. P. Feynman and A. R. Hibbs, *Quantum Mechanics and Path Integrals* (McGraw-Hill, New York, 1965).

[88] V. H. Trinh, O. I. Tolstikhin, L. B. Madsen, and T. Morishita, First-order correction terms in the weak-field asymptotic theory of tunneling ionization, Phys. Rev. A **87**, 043426 (2013).

[89] N. B. Delone and V. P. Krainov, Energy and angular electron spectra for the tunnel ionization of atoms by strong low-frequency radiation, J. Opt. Soc. Am. B **8**, 1207 (1991).

[90] O. I. Tolstikhin, T. Morishita, and L. B. Madsen, Theory of tunneling ionization of molecules: Weak-field asymptotics including dipole effects, Phys. Rev. A **84**, 053423 (2011).

[91] K. Liu, S. Luo, M. Li, Y. Li, Y. Feng, B. Du, Y. Zhou, P. Lu, and I. Barth, Detecting and Characterizing the Nonadiabaticity of Laser-Induced Quantum Tunneling, Phys. Rev. Lett. **122**, 053202 (2019).

[92] D. S. Shafer and Z. Zhang, *Introductory Statistics* (FlatWorld Knowledge, Boston, 2010).

[93] V. H. Trinh, O. I. Tolstikhin, and T. Morishita, Weak-field asymptotic theory of tunneling ionization: benchmark analytical results for two-electron atoms, J. Phys. B: At. Mol. Opt. Phys. **48**, 061003 (2015).

[94] H. Matsui, O. I. Tolstikhin, and T. Morishita, Weak-field asymptotic theory of tunneling ionization of the hydrogen molecule including core polarization, spectator nucleus, and internuclear motion effects, Phys. Rev. A **103**, 033102 (2021).

[95] P. M. Kraus, B. Mignolet, D. Baykusheva, A. Rupenyan, L. Horný, E. F. Penka, G. Grassi, O. I. Tolstikhin, J. Schneider, F. Jensen, L. B. Madsen, A. D. Bandrauk, F. Remacle, and H. J. Wörner, Measurement and laser control of attosecond charge migration in ionized iodoacetylene, Science **350**, 790 (2015).

[96] T. Endo, A. Matsuda, M. Fushitani, T. Yasuike, O. I. Tolstikhin, T. Morishita, and A. Hishikawa, Imaging Electronic Excitation of NO by Ultrafast Laser Tunneling Ionization, Phys. Rev. Lett. **116**, 163002 (2016).

[97] T. Endo, H. Fujise, H. Hasegawa, A. Matsuda, M. Fushitani, O. I. Tolstikhin, T. Morishita, and A. Hishikawa, Angle dependence of dissociative tunneling ionization of NO in asymmetric two-color intense laser fields, Phys. Rev. A **100**, 053422 (2019).

[98] A. J. F. Siegert, On the derivation of the dispersion formula for nuclear reactions, Phys. Rev. **56**, 750 (1939).

[99] J. Humblet, Sur la définition des niveaux virtuels des noyaux atomiques et l'établissement de la formule de dispersion, Mém. Soc. R. Sci. Liège Collect. in-8 **12**, 9 (1952).

[100] J. Humblet and L. Rosenfeld, Theory of nuclear reactions: I. Resonant states and collision matrix, Nucl. Phys. **26**, 529 (1961).

[101] L. O. Krainov, P. A. Batishchev, and O. I. Tolstikhin, Siegert pseudostate formulation of scattering theory: General three-dimensional case, Phys. Rev. A **93**, 042706 (2016).

[102] E. E. Shnol', Remarks on the theory of quasistationary states, Teor. Mat. Fiz. **8**, 140 (1971) [Sov. Phys. Theor. Math. Phys. **8**, 729 (1971)].

[103] Y. B. Zel'dovich, On the theory of unstable states, Zh. Eksp. Teor. Fiz. **39**, 776 (1960) [Sov. Phys. JETP **12**, 542 (1961)].

[104] A. M. Dykhne and A. V. Chaplik, Normalization of the wave functions of quasistationary states, Zh. Eksp. Teor. Fiz. **40**, 1427 (1961) [Sov. Phys. JETP **13**, 1002 (1961)].

[105] N. Hokkyo, A remark on the norm of the unstable state: A role of adjoint wave functions in non-self-adjoint quantum systems, Prog. Theor. Phys. **33**, 1116 (1965).

[106] W. J. Romo, Inner product for resonant states and shell-model applications, Nucl. Phys. A **116**, 617 (1968).

[107] O. I. Tolstikhin, V. N. Ostrovsky, and H. Nakamura, Siegert pseudostate formulation of scattering theory: One-channel case, Phys. Rev. A **58**, 2077 (1998).

[108] N. L. Manakov, M. V. Frolov, A. F. Starace, and I. I. Fabrikant, Interaction of laser radiation with a negative ion in the presence of a strong static electric field, J. Phys. B: At. Mol. Opt. Phys. **33**, R141 (2000).

[109] L. D. Faddeev and S. P. Merkuriev, *Quantum Scattering Theory for Several Particle Systems* (Kluwer Academic, Dordrecht, 1993).

[110] J. D. Dollard, Asymptotic convergence and the coulomb interaction, J. Math. Phys. **5**, 729 (1964).

[111] L.-Y. Peng, E. A. Pronin, and A. F. Starace, Attosecond pulse carrier-envelope phase effects on ionized electron momentum and energy distributions: roles of frequency, intensity and an additional IR pulse, New J. Phys. **10**, 025030 (2008).

[112] O. I. Tolstikhin and C. Namba, Quantum-mechanical and semiclassical study of the collinear three-body Coulomb problem: Inelastic collisions below the three-body disintegration threshold, Phys. Rev. A **70**, 062721 (2004).

[113] J. Wang, J. P. D'Incao, and C. H. Greene, Numerical study of three-body recombination for systems with many bound states, Phys. Rev. A **84**, 052721 (2011).

[114] H. Suno, Y. Suzuki, and P. Descouvemont, Triple-α continuum structure and hoyle resonance of ^{12}C using the hyperspherical slow variable discretization, Phys. Rev. C **91**, 014004 (2015).

[115] A. Simoni, A. Viel, and J.-M. Launay, Application of the spectral element method to the solution of the multichannel Schrödinger equation, J. Chem. Phys. **146**, 244106 (2017).

[116] C. H. Yuen and V. Kokoouline, Jahn-Teller effect in three-body recombination of hydrogen atoms, Phys. Rev. A **101**, 042709 (2020).

[117] J. Svensmark, O. I. Tolstikhin, and T. Morishita, Adiabatic theory of strong-field ionization of molecules including nuclear motion, Phys. Rev. A **101**, 053422 (2020).

[118] C. Bloch, Une formulation unifiée de la théorie des réactions nucléaires, Nucl. Phys. **4**, 503 (1957).

[119] D. O. Harris, G. G. Engerholm, and W. D. Gwinn, Calculation of matrix elements for one-dimensional quantum-mechanical problems and the application to anharmonic oscillators, J. Chem. Phys. **43**, 1515 (1965).

[120] A. S. Dickinson and P. R. Certain, Calculation of matrix elements for one-dimensional quantum-mechanical problems, J. Chem. Phys. **49**, 4209 (1968).

[121] J. C. Light, I. P. Hamilton, and J. V. Lill, Generalized discrete variable approximation in quantum mechanics, J. Chem. Phys. **82**, 1400 (1985).

[122] O. I. Tolstikhin and C. Namba, *CTBC–A Program to Solve the Colinear Three-body Coulomb Problem: Bound States and Scattering Below the Three-body Disintegration Threshold* (National Institute for Fusion Science, Toki, Japan, 2003).

[123] M. Abramowitz and I. A. Stegun, *Handbook of Mathematical Functions with Formulas, Graphs, and Mathematical Tables* (Dover, New York, 1964).

[124] E. P. Wigner and L. Eisenbud, Higher angular momenta and long range interaction in resonance reactions, Phys. Rev. **72**, 29 (1947).

[125] W. H. Press, S. A. Teukolsky, W. T. Vetterling, and B. P. Flannery, *Numerical Recipes in FORTRAN* (Cambridge University Press, Cambridge, 1992).

[126] D. H. Bailey, MPFUN2015: A thread-safe arbitrary precision computation package (full documentation).

[127] E. Anderson, Z. Bai, C. Bischof, S. Blackford, J. Demmel, J. Dongarra, J. Du Croz, A. Greenbaum, S. Hammarling, A. McKenney, and D. Sorensen, *LAPACK Users' Guide*, 3rd ed. (SIAM, Philadelphia, 1999).